X-ray absorption spectroscopic investigation of the Ca and Mg environments in CO2-bearing silicate glasses

Yann Morizet, Nicolas Trcera, Chloé Larre, Marion Rivoal, Erwan Le Menn, Delphine Vantelon, Fabrice Gaillard

Accepted Manuscript

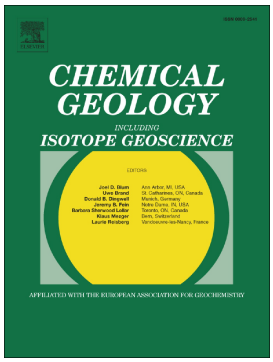

X-ray absorption spectroscopic investigation of the Ca and Mg environments in CO2-bearing silicate glasses

Yann Morizet, Nicolas Trcera, Chloé Larre, Marion Rivoal, Erwan Le Menn, Delphine Vantelon, Fabrice Gaillard

PII: S0009-2541(19)30055-5
DOI: https://doi.org/10.1016/j.chemgeo.2019.02.014
Reference: CHEMGE 19063

To appear in: *Chemical Geology*

Received date: 21 October 2018
Revised date: 10 January 2019
Accepted date: 10 February 2019

Please cite this article as: Y. Morizet, N. Trcera, C. Larre, et al., X-ray absorption spectroscopic investigation of the Ca and Mg environments in CO2-bearing silicate glasses, Chemical Geology, https://doi.org/10.1016/j.chemgeo.2019.02.014

X-RAY ABSORPTION SPECTROSCOPIC INVESTIGATION OF THE CA AND MG ENVIRONMENTS IN CO_2-BEARING SILICATE GLASSES

Yann MORIZET[1*], Nicolas TRCERA[2], Chloé LARRE[1,3], Marion RIVOAL[1], Erwan LE MENN[1], Delphine VANTELON[2], Fabrice GAILLARD[3]

[1] Université de Nantes, Nantes Atlantique Universités, Laboratoire de Planétologie et Géodynamique de Nantes (LPGN), UMR CNRS 6112, 2 rue de la Houssinière, 44322 Nantes Cedex, France

[2] Synchrotron SOLEIL, L'Orme des Merisiers, Saint Aubin, BP 48, F-91192 Gif-sur-Yvette Cedex, France

[3] CNRS – Université d'Orléans – BRGM, UMR 7327, Institut des Sciences de la Terre d'Orléans, 1a rue de la Férollerie, 45071 Orléans, France

Corresponding author: Yann Morizet

Postal address:

Laboratoire de Planétologie et Géodynamique de Nantes (LPG), UMR-CNRS 6112, Université de Nantes.

2 rue de la Houssinière, 44322 Nantes Cedex (FRANCE)

phone: +33 (0) 2 5112 5491

fax: +33 (0) 2 5112 5268

*E-mail: yann.morizet@univ-nantes.fr

Abstract

Recent investigation showed that the CO_2 solubility in silicate melts is strongly affected by the #Mg (MgO/MgO+CaO). CO_2 solubility is decreasing with increasing #Mg implying that CO_2 molecules dissolves in the vicinity of Ca atoms to form CO_3^{2-} molecular groups. We have investigated several CO_2-bearing (up to 17.2 wt.%) silicate glasses using X-ray Absorption Spectroscopy (XAS) at the Mg and Ca K-edge in order to determine the structural environments of Mg^{2+} and Ca^{2+} cations. Analyses of the Mg XANES region show that the Mg environment is not affected by the presence of CO_2 dissolved as CO_3^{2-} groups regardless of the CO_2 content. The Mg K-edge EXAFS simulations and XANES modelling show that the average Mg-O distance is close to 2 Å and the average Mg coordination is close to 6.

On the contrary, the position of the Ca XANES peak main resonance related to first-coordination shell is negatively correlated with the CO_2 content and shifts from 4051.4 to 4050.8 eV with CO_2 increasing from 0 to 17.2 wt.%. The Ca EXAFS simulations showed that Ca-O average distance is longer (~2.5Å) than the Mg-O distance. Furthermore, we observed that the Ca coordination number is positively correlated with the CO_2 content: Ca coordination number increases from 7 to 9 for CO_2 content changing from 0 to 17.2 wt.%.

Mg and Ca XAS results suggest that CO_3^{2-} groups are dissolved in the vicinity of Ca^{2+} cations and not in the surrounding of Mg^{2+} cations which environment remains unaffected by CO_2 dissolution. The tighter Mg atomic environment as well as the lower coordination number for Mg cations as compared to Ca atomic environment could explain such behaviour. One implication of this result is the lower CO_2 transport capacity for Mg-rich silicate melts such as komatiites or kimberlites.

Number of word: 293

Keywords: CO_2 dissolution mechanism, XANES, EXAFS, Mg and Ca structural environment.

1. Introduction

Carbon dioxide (CO_2) is an ubiquitous volatile species involved in many magmatic systems. CO_2 becomes dominant in some volcanic systems having very peculiar magmatic compositions which are low in silica such as melilitites or kimberlites. The study of these natural magmatic occurrences shows that CO_2 is known to dissolve in large quantities typically above 10 wt.% (Kjarsgaard et al., 2009; Russell et al., 2012; Bosshard-Stadlin et al., 2014). Previous experimental investigations (Brey and Ryabchikov, 1994; Brooker et al., 2001; 2011; Moussallam et al., 2015, 2016; Morizet et al., 2017a,b) emphasised that low silica melts such as melilitites and kimberlites are highly efficient in carrying CO_2 from the source at depth to the surface resulting in high CO_2 degassing.

Reconstruction of the CO_2 solubility (i.e. degassing) paths for these silicate melts has benefited from numerous experimental investigations since decades. For instance, the effect pressure and temperature induce on the CO_2 solubility is well-known (e.g. Blank and Brooker, 1994; Thibault and Holloway, 1994; Brooker et al., 1999; Morizet et al., 2002; Moussallam et al., 2015) and is well-reproduced by existing thermodynamic models (Newman and Lowenstern, 2002; Papale et al., 2006; Iacono-Marziano et al., 2012). The impact of redox conditions on CO_2 solubility is more complicated to apprehend (Pawley et al., 1992; Kadik et al., 2004; Morizet et al., 2010; Wetzel et al., 2013; Eguchi and Dasgupta, 2018) and further investigations are necessary to better constrain the CO_2 solubility change with fO_2 variations. Many studies have focused on the effect of silicate melt compositions on CO_2 solubility and several layers of knowledge have to be distinguished. Whereas a clear effect of the SiO_2 content in silicate melt has been demonstrated on CO_2 solubility (Blank and Brooker, 1994;

Brooker et al., 1999; Massuyeau et al., 2015), Brooker et al. (2001) went further and showed that the CO_2 solubility is positively correlated to the increase in the Non-Bridging Oxygen per Tetrahedron ratio (NBO/T) calculated on the stoichiometric basis (Mysen, 1990). This parameter calculated from chemical composition links to the atomic structure and high NBO/T corresponds to a strongly depolymerized structure (i.e. more disrupted network). Therefore, the NBO/T also relates at some point to the CO_2 dissolution mechanisms: at NBO/T = 0, CO_2 will dissolve as CO_2 molecules in fully polymerized compositions (Brooker et al., 1999); at NBO/T < 1, CO_2 will dissolve as network carbonates (Brooker et al., 2001b); NBO/T > 1, CO_2 will form Free Ionic Carbonates (Morizet et al., 2017b,c). However, this is a first order approach as the calculation does not address the possible effect on CO_2 solubility of the cation nature and which was early suspected (Brey and Ryabchikov, 1994; Dixon, 1997); furthermore it only provides a partial picture of the structural molecular units within the glass and the fine molecular structure (i.e. different Al or Mg coordination numbers) is not depicted in the current NBO/T calculation.

The recent experimental work we have conducted aimed at investigating this second order of the effect of silicate melt chemical composition on CO_2 solubility. In two consecutive studies we showed that CO_2 solubility is affected by the #K = K_2O/K_2O+Na_2O (Morizet et al., 2014) and #Mg = MgO/MgO+CaO (Morizet et al., 2017a). The CO_2 solubility in silicate melts increases with increasing #K and decreases with increasing #Mg. Such changes are related to the change in the cation field strength (z/r^2 with z cationic charge and r ionic radius) which increases in the following order $K^+ > Na^+ > Ca^{2+} > Mg^{2+}$. Using a compilation of CO_2 solubility experimental data we have established a global parameter (Melt Ionic Field Strength dependent on the z/r^2) which can predict the maximum CO_2 solubility in a continuum of silicate melt chemical composition from basalt to carbonatite. This result has major implications either on CO_2 degassing in volatile-rich magmatic systems or on the CO_2

transport capability of silicate melts from the mantle source towards the surface. In particular, the impact of the high Mg concentration in natural kimberlite compositions onto CO_2 solubility and CO_2 degassing has never been addressed (Le Roex et al., 2003; Kjarsgaard et al., 2009; Russell et al., 2012; Kamenetsky et al., 2013), because most of the available experimental investigations have focused on Mg-poor silicate melt compositions.

One reason for the lower CO_2 solubility in Mg-rich silicate melt compositions is to be found in the CO_2 dissolution mechanisms into the melt structure. It has been demonstrated from NMR investigation that in low silica melts CO_2 dissolution uses available NBOs from the silicate network to form CO_3^{2-} molecular groups which are totally disconnected from the silicate network and called Free Ionic Carbonates (FIC, Morizet et al., 2017b, c) in agreement with the early theory for CO_2 dissolution mechanisms (Eggler, 1978; Mysen and Virgo, 1980). Considering that CO_2 solubility was decreasing with increasing Mg content therefore it was suspected that CO_2 dissolves in the vicinity of Ca^{2+} cations forming $Ca^{2+}..CO_3^{2-}$ FIC. However, the preferred CO_2 dissolution in the surrounding of Ca^{2+} cations instead of Mg^{2+} cations remained to be explained. The present goal of this work is to determine if such CO_2 affinity is due to a difference in the structural environment of Ca^{2+} and Mg^{2+} or just a difference in the thermodynamic affinity.

Ca and Mg in silicate melts have similar behaviour and act principally as network modifying cations. However, in details, the structural environment of Mg^{2+} is different from the Ca^{2+} one reflecting the difference in the cation field strength. Most of the structural information on the atomic environments of these two elements was gathered from X-ray diffraction/absorption, neutron scattering and Solid-State Nuclear Magnetic Resonance (NMR); however, NMR spectroscopy reveals itself limited in providing structural information on these two particular elements. The extremely broad signal obtained from ^{25}Mg NMR in silicate glasses (Fiske and Stebbins, 1994; Kroeker and Stebbins, 2000; Shimoda et al., 2007) does not allow to fully

characterizing the Mg atomic environments and the clear discrimination of the Mg coordination in silicate glasses using ^{25}Mg NMR spectroscopy is still to be improved. The expensive nature of the NMR active ^{43}Ca isotopes has limited the number of structural investigations on that element (Angeli et al., 2007; Gambuzzi et al., 2015).

Mg and Ca X-ray Absorption Spectroscopy (XAS) have proven to be efficient in determining the atomic environment of these elements present either in minerals (e.g. Ildefonse et al., 1995; Paris et al., 1995; Andrault et al., 1998; Cabaret et al., 1998; Mottana et al., 1999; Quartieri et al., 2008; Fleet and Liu, 2009; Trcera et al., 2009; Yoshimura et al., 2013; Blanchard et al., 2016) or in silicate glasses (Taniguchi et al., 1997; Cormier and Neuville, 2004; Neuville et al., 2004; Guignard and Cormier, 2008; Trcera et al., 2009; 2011; Moulton et al., 2016; Ragoen et al., 2017). The application of Mg and Ca X-ray Absorption Near-Edge Spectroscopy (XANES) to a large variety of minerals has allowed establishing empirical curves for the Ca-O (Sowrey et al., 2004) and Mg-O (Li et al., 1999) coordination environments. Furthermore, the combined approach on both minerals and silicate glasses are often used to qualitatively determine the Ca and Mg structural environments in silicate glasses (Cormier and Neuville, 2004; Trcera et al., 2009). As for Extended X-ray Absorption Fine-Structure (EXAFS), it is currently applied to silicate glasses to determine 1) element coordination and 2) spatial relationship with nearest neighbours (Binsted et al., 1985; Jackson et al., 2005; Newville, 2014; Mastelaro and Zanotto, 2018). The recent study of Pohlenz et al. (2018) is the only one to show that the presence of CO_2 molecules affects the average distance to oxygen for strontium and lanthanum. If the change in cationic structural environment as a function of the silicate glasses bulk chemical composition has been widely studied; up to now, no investigation was conducted on the effect of CO_2 onto the Mg or Ca cationic environments in silicate glasses using XAS.

In the present study, we investigated the change in Ca and Mg structural environments in CO_2-bearing silicate glasses using XAS (XANES and EXAFS). We studied silicate glasses with various compositions (from kimberlite to basalt) previously reported and having CO_2 concentrations up to 17 wt.%. As suspected, we observed that the Mg XANES in all investigated glasses is not affected by the presence of CO_2. On the contrary, the Ca XANES spectra exhibit changes in peak positions with increasing CO_2 content which can be interpreted as a change in the Ca structural environments upon CO_2 dissolution. We conducted the analyses of the EXAFS spectra in order to extract the Ca and Mg structural parameters (bond length and coordination number to oxygens). A discussion is proposed in order to explain the CO_2 preferred dissolution in the surrounding of Ca^{2+} and not Mg^{2+} cations.

2. Experimental method

2.1 CO_2-bearing silicate glasses

The elemental composition of the investigated glasses is reported in Table 1. The studied glasses are CO_2-bearing silicate glasses with CO_2 content from 1.5 to 17.2 wt.%; an additional CO_2-free wollastonite glass ($CaSiO_3$) has been also studied for Ca environment, hence constraining the effect of CO_2 onto the Ca atomic environment. In all the investigated glasses, the CO_2 content has been determined using Raman spectroscopy and the method of Morizet et al. (2013). The accuracy on the determined CO_2 is 10% in relative to the value. The CO_2-bearing silicate glasses were synthesised under high pressure conditions using piston-cylinder apparatus between 0.5 and 3.0 GPa for pressure and at temperature above 1400°C. The CO_2-free wollastonite glass has been prepared in a Pt crucible placed in a 1 atm vertical furnace at 1500°C for several hours. Except for the TA series, the investigated glasses were studied

previously and the details of the synthesising method can be found in the subsequent publications. Most of the glass compositions are Fe-free in the Na_2O-CaO-MgO-Al_2O_3-SiO_2 system. The RB8, HK, X and βMDE-5 were studied and reported in Morizet et al. (2017a). The TA samples are newly synthesised CO_2-bearing glasses and were prepared from a natural peralkaline lamprophyre from Torre Alfina (Fe-bearing, Mitchell, 1989) to which carbonate ($CaCO_3$, Na_2CO_3, $CaMg(CO_3)_2$ and K_2CO_3; as a source of CO_2) and oxides (SiO_2, Al_2O_3 and MgO) were added to attain the TA12 and TA10b major element compositions. TA12-C1, -C3 and TA10b-C1, -CH1 powders were loaded into Pt capsule and CO_2-bearing glasses synthesised at pressure of 1.0 and 3.0 GPa using ½ inch piston-cylinder assemblies; temperature was set to 1400°C and monitored with type B thermocouple. The run duration was 30 min and the rapid quench (>100°C/s) was conducted by cutting-off the power at the end of the experiment.

The investigated compositions are depolymerized in nature. For instance, the NBO/T ranges from moderately depolymerized (NBO/T ~1) for βMDE-5 to strongly depolymerized (NBO/T > 3) for HKM and TA10b samples. One reason for studying depolymerizing silicate glass compositions is that these compositions dissolve a large amount of CO_2 in their structure (see Table 1) and the way CO_2 dissolves into the silicate melt structure is well-constrained (Brooker et al., 1999, 2001; Morizet et al., 2015, 2017a,b,c). We also reported the value of #Mg; considering that the concentration of Mg in glass has been inferred to be a major control of the CO_2 solubility (Morizet et al., 2017a).

The investigated database regroups samples synthesised at different pressure (up to 3.0 GPa), showing various CO_2 content (up to 17.2 wt.%), having different #Mg (up to 0.67); and different degrees of polymerization (i.e. 1 < NBO/T < 3.4). Hence, considering the large variety of glass samples, we expect to extract the effect of pressure, the effect of NBO/T and

#Mg on cation atomic environments, and by extension the CO_2 dissolution mechanisms and its effect on cation atomic environments.

2.2 XAS measurements

Mg and Ca K-edges XAS (EXAFS and XANES) spectra were collected on LUCIA beamline at SOLEIL synchrotron (Flank et al., 2006; Vantelon et al., 2016) using KTP and Si(111) monochromator, respectively. We used silicon drift diode detector and the spectra on the glass were acquired in fluorescence mode. Energy calibration was performed according to the Mg K-edge of periclase and Ca K-edge of diopside, respectively. The incoming beam size was 3x5 mm^2. The samples were stick to a copper plate mounted onto an indium foil or with silver lacquer. The sample orientation had a 30° angle normal to the detector in order to increase the signal to noise ratio. Mg XANES spectra had to be corrected from self-absorption. We used the Athena Self-Absorption tool (Ravel and Newville, 2005) to do so. No self-absorption correction was needed for Ca XANES spectra.

The Mg XANES and EXAFS spectra were collected in the range 1250-1300 eV with a step of 2 eV, in the range 1300-1322 eV with a step of 0.1 eV, in the range 1322-1338 eV with a step of 0.5 eV and in the range 1338-1565 eV with a step of 1 eV. The Ca XANES and EXAFS spectra were collected in the range 3920-4035 eV with a step of 2 eV, in the range 4035-4070 eV with a step of 0.1 eV, in the range 4070-4125 eV with a step of 0.5 eV, in the range 4125-4500 eV with a step of 1 eV, in the range 4500-4800 eV with a step of 2 eV and in the range 4800-5000 eV with a step of 3 eV. At least two spectra were acquired on each sample in order to obtain a better signal to noise. The spectra were averaged using the Athena software (Ravel and Newville, 2005). The minimum counting time was set at 1s per point. In the present work the nomenclature for the spectra interpretation and peak assignments is the following: we used

italic capital letters for the peaks in crystalline material and small letters for the peaks in CO_2-bearing silicate glasses.

In addition to the acquisition of the Mg and Ca K-edges XAS spectra on glass, several acquisitions were done on crystalline materials for comparison and fingerprinting. Mg K-edge spectra were collected for spinel ($MgAl_2O_4$), periclase (MgO), diopside ($CaMgSi_2O_6$) and San Carlo olivine (Mg_2SiO_4). In these crystalline compounds the Mg environment varies from 4-coordinated to 6-coordinated, covering the usually observed coordination number for Mg in silicate glasses (Taniguchi et al., 1997; Li et al., 1999; Kroeker and Stebbins, 2000; Kohara et al., 2004; Trcera et al., 2009; 2011; Wilding et al., 2012). Ca K-edge spectra for crystalline calcite ($CaCO_3$), dolomite ($CaMg(CO_3)_2$), diopside ($CaMgSi_2O_6$) and anorthite ($CaAl_2Si_2O_8$); therefore covering a large range of Ca coordination from 6 to 12, also in agreement with the usually considered Ca coordination number in silicate glasses (Taniguchi et al., 1997; Cormier and Neuville, 2004; Shimoda et al., 2008; Cormier and Cuello, 2013; Cicconi et al., 2016).

The acquired spectra were background subtracted using a polynomial function below the edge and then spectra were normalized in the EXAFS region using a cubic function. The EXAFS region could be turned into k space ($\chi(k)$). For the EXAFS analyses, we used k^2- and k^3-weighted for Ca and Mg spectra, respectively. The simulation of the EXAFS region was done with the Artemis software and the DEMETER package (Ravel and Newville, 2005). The simulations were conducted in order to obtain the average distance to oxygen as well as the coordination number to oxygens; which are contained in the EXAFS signal for the first coordination sphere.

For the Mg EXAFS, the simulation is conducted with k ranging from 2 and up to 7 $Å^{-1}$ and R ranging from 1 and up to 2.2 Å. To simulate the Mg EXAFS of the CO_2-bearing silicate

glasses, we used a single scattering path Mg to O from periclase standard crystalline structure: Coordination Number (CN) = 6, R_{Mg-O} = 2.11 Å. Because of the low number of independent points computed from the Fourier transform and fitting range, it was more appropriate from statistical point of view to only use a single path. Furthermore, simulations lead to relevant results and additional results were not necessary. Prior the simulation, the Mg EXAFS spectrum for periclase was simulated with theoretical single scattering factors obtained from a periclase crystallographic structure. We obtained the scattering amplitude S_0^2 = 0.85 and a refined value of the E0 (ΔE0 = -2.06 eV). We kept these values for the simulation of the silicate glasses EXAFS spectra.

For the Ca EXAFS, the simulation is conducted with k ranging from 2 to 8 $Å^{-1}$ and R ranging from 1 to 3 Å. We used several single scattering paths Ca to O from diopside to extract the first coordination sphere: O_1, Coordination Number (CN) = 4, R_{Ca-O} = 2.36 Å; O_2, CN = 2, R_{Ca-O} = 2.56 Å; O_3, CN = 2, R_{Ca-O} = 2.72 Å and a single scattering path Ca to Si: CN = 2, R_{Ca-Si} = 3.09 Å. Prior to the simulation of the spectra for silicate glasses we conducted a simulation on the Ca EXAFS spectrum obtained on standard crystalline diopside and obtained the scattering amplitude S_0^2 = 0.977 and the ΔE0 = 1.93 eV. Due to the low number of independent points (~5 for 9 parameters), the optimization was accomplished in several steps: the average d_{Ca-O} for each path was optimized then followed by the optimization of the Debye-Waller attenuation factor for each path and finally an optimization of the coordination number (CN) was performed. The initial guesses were 0 for the deviation in the d_{Ca-O}, 0.003 for the Debye-Waller parameter and 4, 2 and 2 for the CN corresponding to the initial CN of the single scattering in the crystalline diopside. The three steps of the optimization were repeated several times in order to obtain a robust simulation of the EXAFS oscillation in k- and R-space. Considering that we keep the S_0^2 and the ΔE0 constant for both Mg and Ca EXAFS simulations therefore simulation results for silicate glasses can be compared in

relative to each other and the effect CO_2 could induce on the Mg and Ca atomic environments deciphered.

3. Results

Typical Mg and Ca K-edges spectra are shown in Figure 1 and 2, respectively. The entire set of spectra can be found in Supplementary material. Spectra for CO_2-bearing silicate glasses are collated along with spectra for crystalline materials: periclase and spinel for Mg, dolomite and diopside for Ca. The spectra for CO_2-bearing silicate glasses are categorized: A, for kimberlite or melilitite with NBO/T > 2; B, haplobasalt with NBO/T = 1, P = 1.5 GPa.

3.1 Mg XAS spectra

The line shape of the Mg spectra in the XANES region for CO_2-bearing glasses is different from the one in crystalline standards as seen in Figure 1. The Mg spectra in the XANES region are consistent with previous works for crystalline material (Ildefonse et al., 1995; Cabaret et al., 1998; Neuville et al., 2009; Trcera et al., 2009; 2011) and for Mg-bearing silicate glasses (Curti et al., 2009; Trcera et al., 2009; 2011; Moulton et al., 2016). Typically, the spectrum obtained for spinel is composed of three sharp peaks located at 1309.1, 1314.3, 1318.5 eV and two broad peaks at 1332 eV and 1350-1375 eV. The different peaks are denoted as *A, B, C, D* and *E* respectively (following the commonly used nomenclature, Trcera et al., 2009). For periclase, the same peaks can be retrieved but at different absorption energy: the *D* and *E* peaks are shifted to lower energy whereas the *A* peak is shifted to higher energy. Both spectra do not show any evidence of pre-edge peak such as the one observed for enstatite and pyrope (Figure 1B, Trcera et al., 2009). The lower energy for *D* and *E* peaks in periclase than for spinel would be related to the higher Mg coordination number for periclase than for spinel (Trcera et al., 2009).

For CO_2-bearing silicate glasses in Figure 1, we observe that the XAS spectrum line shape is similar in between the investigated samples and comparable to previously reported spectra for silicate glasses (Ildefonse et al., 1995; Curti et al., 2009; Trcera et al., 2009; 2011; Moulton et al., 2016). The Mg spectrum in the XANES is a composition of several components and does not show pre-edge feature. The four peaks labelled *a* to *d* can be identified for silicate glasses (Li et al., 1996, Moulton et al., 2016). The comparison with crystalline spectra shows that the peak *C* and *D* are merged into *c* peak; and the latter is not always clearly observed for silicate glasses on the contrary to crystalline compounds. An assignment of these peaks has been proposed in previous work and attributed to different electronic transition: *a* peak is assigned to 1s to empty 3p; *b* and *d* peaks are related to the first coordination shell of Mg atoms, 1s $\rightarrow$ 3p first coordination shell electronic transition for *b* and first shell resonance of the Mg-O coordination for *d*; peak *c* is related to multiple scattering from coordination spheres around the absorbing Mg (Cabaret et al., 1998; Ildefonse et al., 1998; Li et al., 1999; Trcera et al., 2009; Moulton et al., 2016).

In between the Mg XAS spectra of the different CO_2-bearing sample, the differences are not clearly visible. For instance, in Figure 1A, the spectra line shape is similar for the natural kimberlite TA10b-C1 and the synthetic kimberlite (HK). HK-3 spectrum appears slightly different from the other HK samples; this difference is not clearly explained: it could be due to an analytical artefact or it could be inherent to the sample itself and the presence of nano-crystals. Except for this particular sample, the HK sample spectra are similar in shape; the position of the labelled *a*, *b*, *c* and *d* appears comparable even though the samples have been synthesised at different pressure and have different CO_2 content.

For the haplobasalt compositions, the main difference observed is on the *a* and *b* peaks in between X1-2 and X3-2 spectra. There is a substantial increase in the *a* peak from X1-2 to X3-2 whereas the *b* peak appears to decrease in relative intensity. The main difference in

between these samples is #Mg which varies from 0.25 to 0.67 in between X1-2 and X3-2. Previous works (Trcera et al., 2009; Moulton et al., 2016) showed that the change in the *a* peak intensity could be related to the Mg content with an increase in the *a* peak intensity with decreasing Mg content. In Figure 1B, surprisingly it appears to be the other way around with an increase in the *a* peak with increasing Mg content. It can be suggested that there is a change in the Mg environment not related to the Mg content itself but to another factor. Considering that those samples have been synthesised at identical pressure (1.5 GPa) and that it is difficult to relate such a change with the Mg content, therefore the observed change is currently unexplained. Although, there is a difference in the CO_2 content (from 1.5 to 7.5 wt.%), it appears highly speculative to suggest that CO_2 is responsible for the change in the spectrum line shape as it has only been observed for these two particular samples. Notwithstanding, the change in the peak *a* intensity might correspond to a change in the Mg-O bond length and polyhedral distortion (Cabaret et al., 1998; Li et al., 1999; Trcera et al., 2009; 2011; Moulton et al., 2016).

Using the crystalline standards as a fingerprint to decipher the Mg environment in silicate glasses is currently difficult. The investigated silicate glasses exhibit Mg XANES spectra showing features which can be found in both the crystalline spinel and periclase spectra. For example, the *A* peak prominent in spinel spectrum is also visible in the periclase one but at slightly higher energy and the *a* peak in silicate glasses can be a combination of both. Similarly, peak *c* or *d* in silicate glasses are broad and could represent a combination of several Mg environments ranging from 4- to 6-coordinated as inferred by previous works (Wilding et al., 2012). However, one common aspect in between the Mg XAS spectra for CO_2-bearing silicate glasses is that CO_2 content does not appears to induce a dramatic change on the Mg atomic environments. This is consistent with our current idea that CO_2 molecules

do not dissolve in the vicinity of Mg^{2+} cations or only to a limited extent and CO_2 molecules will have stronger interactions with Ca^{2+} or Na^{+} cations (Morizet et al., 2017a).

3.2 Ca XAS spectra

The Ca XAS spectra are presented in Figure 2 showing the XANES and EXAFS regions. Ca XAS spectra for crystalline dolomite and diopside are comparable to previous work (Cormier and Neuville, 2004; Blanchard et al., 2016). In a similar way to the Mg XAS spectra, within each category of silicate glasses (Figure 2), the differences in between the Ca XAS spectra are weak and all spectra show almost identical line shape in the XANES and EXAFS regions. As a result, the possible effect CO_2 will induce on the Ca environment in silicate glass will be difficult to establish. The method of fingerprinting with crystalline standard to investigate the effect CO_2 will induce on the Ca atomic environment will also be limited as very subtle changes are suspected. The Ca XAS spectra for crystalline compounds and silicate glasses show the evidence of a pre-edge peak around 4040 eV (*p*) which corresponds to a 1s $\rightarrow$ 3d type transition (Combes et al., 1991; Cormier and Neuville, 2004). The pre-edge peak is present in all spectra of silicate glasses regardless of the CO_2 content. The main resonance (*b*, assigned to 1s $\rightarrow$ n p transition) is observed at ~4051 eV for the silicate glasses. For crystalline compounds, the peak maximum position varies from 4048 to 4050 eV for dolomite and diopside, respectively. A first comparison in between Ca XAS for silicate glasses and minerals suggests that the Ca environments in silicate glasses is probably closer to the one in diopside than in dolomite; however, the presence of the shoulder (*a*) for Ca XAS spectra in silicate glasses before the main line could be explained by a possible combination of both Ca environments: 6- and 8-coordinated Ca (Skinner et al., 2012; Cormier and Cuello, 2013; Gambuzzi et al., 2015). Furthermore, the examination of the first EXAFS oscillation in

silicate glasses (*c*, broad peak above 4075 eV) also indicates that the Ca atomic environments in CO_2-bearing silicate glasses is complex and a combination of multiple environments as inferred in previous works (Cormier and Cuello, 2013).

4. Discussion

4.1 Calcium and magnesium atomic environments from XANES in CO_2-bearing silicate glasses

We have investigated the Mg and the Ca XANES region with a particular attention to determine the position of the main line peak maximum (*b* in Figure 1 and 2) as a function of the CO_2 content. The results are reported in Table 2 and represented in Figure 3. The main line peak for Mg is related to the first coordination shell; the same applies to the Ca main line which is related to the 1s $\rightarrow$ n p transition associated to the first coordination shell. Therefore any sort of correlation with the CO_2 content could indicate to some extent a relationship between the CO_2 dissolution mechanism and the investigated atomic environment.

In Figure 3, the same scaling (1 eV) is considered for the Mg and Ca peak maximum and the error on the peak determination is ±0.1 eV. We observe that the main line peak maximum for Ca is negatively correlated to the CO_2 content. The peak maximum changes from 4051.4 eV for CO_2-free Woll glass to 4050.8 eV for HKM sample with 13.2 wt.% CO_2. The negative correlation appears to be non-linear. Although, there is a significant scatter at high CO_2 content; the observed changes are above the possible analytical error (±0.1 eV in this region). The change in the peak position appears not correlated to other parameters such as pressure or NBO/T. For instance, βMDE-5 and X3-2 samples synthesised at 2.0 and 1.5 GPa, respectively; show almost identical peak position at ~4051.2 eV for comparable CO_2 content.

For the HK series at constant NBO/T ~ 2.5, there is a change in the peak position from 4050.9 to 4051.1 eV from HK-1 to HK-2.

Although we did not analyse a CO_2-free Mg-bearing silicate glass, we believe that there is not a similar trend for Mg main resonance and within error, the Mg peak maximum of the Mg XANES spectra remains constant with increasing CO_2 content. For example, the change in the peak maximum does not exceed 0.3 eV from 1.5 (X3-2) to 13.2 wt.% CO_2 (HKM). Whereas a clear change is observed for the Ca XANES peak maximum with increasing CO_2 content, the Mg XANES peak maximum does not seem to be affected by the presence of CO_2 in the silicate glass structure. Therefore, the CO_2 dissolution influences the Ca atomic environment whereas the Mg atomic environment remains unaffected in the silicate glass structure. This observation appears consistent with our previous work showing that 1) increasing the Mg content in silicate melt composition induces a decrease in the CO_2 solubility and 2) CO_2 molecules dissolve preferentially in the vicinity of the Ca^{2+} ionic environments (Morizet et al., 2017a).

We used the model of Li et al. (1999) using the Mg XANES spectra to constrain the Mg local structural environment in the investigated CO_2-bearing silicate glasses and propose a possible coordination environment of the Mg atoms. The model of Li et al. (1999) uses the position of the *a* peak (Figure 1) to constrain the Mg-O distance in Å. The *a* peak line position was determined through the simulation of the Mg XANES spectra for both crystalline compounds and silicate glasses. Typical Mg XANES deconvolutions are provided in Supplementary material and results of the Li et al. (1999) model are shown in Figure 4. The position of the *a* line from the simulation is reported in Table 2 for silicate glasses and the corresponding Mg-O distance (d_{Mg-O}) has been calculated with the equation given by Li et al. (1999). For the crystalline compounds, the *a* line was determined at 1309.2, 1310.09 and 1310.60 eV for spinel, periclase and diopside, respectively. The corresponding calculated d_{Mg-O} is 1.92, 1.99

and 2.02 Å. These values are in close agreement with previous works (Ildefonse et al., 1995; Li et al., 1999; Trcera et al., 2009). However, the energy of the *a* line is in contrast with the results obtained by Ragoen et al. (2018) for similar crystalline compounds. Ragoen et al. (2018) derived energy values for the *a* peak which is lower than the one determined in the present study: they determined an energy of ~1307.5 eV for diopside which is 3 eV below the one we obtained. This difference is possibly ascribed to an analytical measurement or simply difference in the studied crystalline materials.

The *a* line values derived for the silicate glasses are comprised in between the values determined for spinel and diopside and change from 1309.4 to 1310.4 eV for TA10b-CH1 and HKM, respectively (see Table 2). The d_{Mg-O} calculated ranges from 1.94 to 2.01 Å. The d_{Mg-O} values are in agreement with the determined values for silicate glasses based on different methods (Wilding et al., 2004; 2008; 2012; Shimoda et al., 2008; Kohara et al., 2011; Cormier and Cuello, 2013). In the investigated silicate glasses (Figure 4), the d_{Mg-O} values do not appear to be correlated to the CO_2 content. For example, the TA10b samples have high CO_2 content (>12 wt.%) and show a d_{Mg-O} at 1.94 Å; and the HKM sample has CO_2 content at 13.2 wt.% and have a d_{Mg-O} at 2.01 Å. Again, this observation tends to confirm that Mg environment changes are not due to the CO_2 dissolution considering that both d_{Mg-O} extrema show high CO_2 content. The origin of the change in d_{Mg-O} is not clearly established in the present work; however it can be due to several parameters such as synthesis conditions (i.e. pressure conditions; Wilding et al., 2012), the silicate glass chemical composition itself (Guignard and Cormier, 2008; Cormier and Cuello, 2013; Moulton et al., 2016) or the structural unit connectivity within the glass (corner- or edge-sharing; ring or non-ring configuration) and the nature of oxygens (BO and/or NBO) surrounding the Mg cations (Kohara et al., 2011). Notwithstanding, the observed range in the d_{Mg-O} is in favour of a multiple Mg coordination environment as inferred by previous works for silicate glasses

(Cormier and Cuello, 2013; Ragoen et al., 2018). Similarly, Kohara et al. (2011) showed that the d_{Mg-O} is related to the chemical strength which can be by extension ascribed to a change in the coordination number of Mg. According to Kohara et al. (2011), at d_{Mg-O} ~2 Å, the chemical strength relatively high indicative of a strong ionic bond to Mg^{2+} cation.

4.2 Magnesium atomic environments from EXAFS in CO_2-bearing silicate glasses

The structural refinement of the Mg EXAFS reduced data for silicate glasses was conducted in order to obtain an estimate of the first coordination sphere of the Mg atoms: average coordination to oxygen atoms and average Mg-O bond length. Typical extracted Mg EXAFS obtained by Fourier transform of the k-weighted ($k^3 \chi(k)$) oscillatory signal is shown in Figure 5 for HKM and X3-2. Because of the limited Mg EXAFS energy range (i.e. limited by Al absorption edge at ~1560 eV), the range in k-space to investigate the fine Mg environments is reduced. In Figure 5, the simulation of the signal has been limited in the range 2.0 to 7.0 $Å^{-1}$ in k-space and 1.0 to 2.2 Å for radial distance R.

Results of the simulation for the CO_2-bearing silicate glasses are reported in Table 2. The d_{Mg-O} from EXAFS varies from 1.98±0.00 to 2.04±0.05 Å for X1-2 and HK1, respectively. The derived d_{Mg-O} values from EXAFS are consistent with the derived values from XANES and the model of Li et al. (1999); however, the value extracted from EXAFS data is longer than the one extracted from XANES data (see Table 2). Similar to XANES, the change in the d_{Mg-O} value appears uncorrelated to the CO_2 content confirming the initial hypothesis that CO_2 does not dissolve in the surrounding of Mg atoms and does not influence the atomic environment of Mg atoms. On average, the d_{Mg-O} is 2.00±0.02 Å and this value is in agreement with previous works on silicate glasses. For example, Guignard and Cormier (2008) derived Mg-O bond length between 1.98 and 2.05 Å for glasses synthesised in the $MgO-Al_2O_3-SiO_2$ system

at 1 bar. Based on Ab Initio Molecular Dynamic simulations, Vuilleumier et al. (2009) determined comparable value for d_{Mg-O}. The derived coordination number for Mg atoms for silicate glasses is also shown in Table 2. The Mg coordination varies from 3.7±1.3 to 6.5±0.9 for HK1 and TA10b-CH1. It should be pointed out that the derived Mg coordination for HK1 has a large error associated with a moderately satisfactory simulation (see Supplementary material). The coordination value of 3.7±1.3 appears anomalously low considering that in silicate glasses Mg atoms adopts a complex structural environment corresponding to a mixture of several structural environments ranging from 4 to 7 in coordination (Cormier and Cuello, 2013). Except for this outlier, all the derived coordination for Mg is consistent with previous investigations for silicate glasses. For instance, Wilding et al. (2012) determined an increase in the Mg coordination number from 4.6 to 5.7 for MgO-SiO_2 glasses with increasing pressure from 1 bar to 8.6 GPa. The varying coordination number for Mg atoms suggests that there is a mixture of Mg atom environments with different coordination ranging from 4 to 7 as inferred in previous works (Trcera et al., 2009; Shimoda et al., 2008b; Vuilleumier et al., 2009; Kohara et al., 2011; Wilding et al., 2012; Cormier and Cuello, 2013). We applied the bond valence theory equations from Brese and O'Keefe (1991) to estimate the Mg coordination number. The Mg valence (ν_{Mg-O}) is related to the bond length d_{Mg-O} with the following equation:

$$\nu_{Mg-O} = \exp\left(\frac{R_{Mg-O} - d_{Mg-O}}{b}\right) \qquad \text{Eq. 1}$$

Where R_{Mg-O} is the bond valence parameter and is 1.693 for Mg and O; b is a constant 0.37 (Brese and O'Keefe, 1991). The coordination number for Mg can be extracted considering the Mg cation charge: CN = 2 / ν_{Mg-O}. The CN for Mg using the d_{Mg-O} obtained from the XANES is slightly lower than the one obtained using the d_{Mg-O} obtained from the EXAFS: CN is comprised between 3.9 and 4.7 from XANES whereas CN is comprised between 4.3 and 5.1

from EXAFS. This latter range is in better agreement with the CN determined using the Mg EXAFS spectrum simulations, although it is slightly lower. Concluding if such small difference is due to the possible dissolution of CO_2 as CO_3^{2-} in the surrounding of Mg atoms is currently not conceivable. We did not observe any correlation between the Mg coordination number and the CO_2 content. We obtained a coordination of 5.6±0.4 for βMDE-5 with 1.7 wt.% CO_2 and an identical coordination of 5.7±0.6 for HKM with 13.2 wt.% CO_2. Hence, within error, all the investigated glasses have comparable Mg atomic environments (average Mg coordination = 5.7±0.7) regardless of the CO_2 content.

Recent atomistic investigations for molten carbonate structure (Vuilleumier et al., 2014; Du et al., 2018) showed that the pair-distribution function for C-O bond has distance below 2 Å; however, from geometrical consideration a CO_3^{2-} molecular group will have a size exceeding the empty space surrounding the Mg atoms in silicate glasses as determined from EXAFS. Reverse calculation of the bond valence theory to derive a d_{Mg-O} value from the Mg CN extracted from EXAFS simulations lead to d_{Mg-O} values close to 2 Å. Furthermore, Kohara et al. (2011) suggest that the empty space in an Mg-rich glass will be close to 0 considering that MgO_x polyhedra will organize with a ring corner-shared structure hence substantially decreasing the free volume within the glass structure. As a result, one possible explanation for the absence of CO_2 dissolution in the vicinity of Mg^{2+} cations is likely to be related to the size of empty space or free volume for accommodating CO_2 molecules in the melt structure.

4.3 Calcium atomic environments from EXAFS in CO_2-bearing silicate glasses

As shown earlier (Figure 3), the analysis of the Ca XANES spectra for silicate glasses points towards an effect of the CO_2 dissolution on the Ca environments. In a similar way to Mg, we treated the Ca EXAFS spectra for the investigated silicate glasses in order to determine the

average bond length in between the Ca atoms and the first nearest neighbour (d_{Ca-O}) and provide an estimate of the Ca coordination number.

We show in Figure 6 the typical simulated Ca EXAFS spectra in k- and R-space. It can be observed that the EXAFS oscillation in k-space is well-reproduced up to 8 $Å^{-1}$. In the range 1.0-3.0 Å, the radial distribution for the first Ca coordination shell is also adequately simulated. The derived average d_{Ca-O} (corresponding to the sum of d_{Ca-O} normalized to the coordination number) is 2.51±0.41 and 2.53±0.43 Å for TA12-C3 and X3-2, respectively. The whole set of derived d_{Ca-O} is given in Table 2. The calculated range of d_{Ca-O} is 2.48 to 2.55 Å for TA12-C1 glass and RB8-2 samples, respectively. The average error on the d_{Ca-O} determined from error propagation on the different single scattering d_{Ca-O} is ±0.32 Å which prevents from determining the real impact of the CO_2 dissolution on the Ca-O bond length in the first coordination shell; hence because of this large error the d_{Ca-O} appears constant regardless of the CO_2 content. According to Sowrey et al. (2004) such a range in d_{Ca-O} would correspond to an increase in the Ca CN of 2.

Studying the Ca coordination values derived from the simulation (see Table 2) reveals that there is an increase in the Ca CN with increasing CO_2 content. This increase is reported in Figure 7. Although the simulation of the Ca EXAFS spectra is probably not unique and the associated error in the EXAFS simulation is rather large, we observe that the Ca coordination number for CO_2-free Woll glass is almost 2 units below the coordination number determined for CO_2-bearing silicate glasses: 7.1±0.5 for Woll glass and 9.5±1.1 for RB8-2. Nevertheless, the coordination value for Woll glass that we determined is probably overestimated; Taniguchi et al. (1997) reported a Ca coordination of 5.6 with a d_{Ca-O} of 2.49 Å from EXAFS measurements; and more recently Skinner et al. (2012) reported a Ca coordination of 6 in wollastonite glass. Early work by Binsted et al. (1985) inferred that the change in Ca CN could be related to the presence of Mg which would increase the Ca CN. In the investigated

glasses, the increase in the Ca CN is independent of the Mg content and is attributed to the presence of CO_2 dissolved as CO_3^{2-}. For instance, we determined an increase in Ca CN from 7.1 to 9.3 in two Mg-free silicate glasses: Woll glass and RB8E-3. The increase in the Ca CN appears not correlated to an increase in the d_{Ca-O} distance as inferred from atomistic calculations from Katz et al. (1996) who showed that an increase in the Ca CN upon hydration is positively correlated to the increase in d_{Ca-O}. The results of Sowrey et al. (2004) also showed that an increase of 2 units in the Ca coordination number would be accompanied by an increase in d_{Ca-O}. In the present work, we do not obtain a sufficient accuracy in the determined d_{Ca-O} to make the same conclusion (see Supplementary material).

Surprisingly, the increase in the Ca coordination value in Figure 7 appears non-linear with a strong increase in the Ca CN then followed by a plateau starting at ~5 wt.% CO_2. This increase does not result from a change in the synthesis conditions (i.e. pressure) or the CaO content of the studied glasses as the higher Ca coordination values (~9) are observed for samples synthesised at various pressures (from 0.5 to 3.0 GPa) and with various CaO content (from ~15 to 40 wt.%). Furthermore, Mountjoy (2007) showed that the increase in Ca CN is only limited in the covered range of pressure. Consequently, the observed change in the Ca coordination number is ascribed to the dissolution of CO_2 molecules in the surrounding of the Ca atoms. However, the observed non-linearity in Figure 7 is currently not explained; whether this increase is due to the type of CO_2 dissolution mechanism is still to be clarified. Morizet et al. (2017b,c) showed that the CO_2 dissolution as Free Ionic Carbonates molecular groups is accompanied by a strong rearrangement of the silicate network structure (i.e. Q^n distribution). One hypothesis is that the dissolution of the CO_2 molecules and the corresponding Q^n change reach an optimal favoured energetic configuration to explain the plateau; however, further work such as First Principle Molecular Dynamic simulations (e.g. Vuilleumier et al., 2009) or Reverse Monte Carlo simulations (e.g. Cormier and Cuello, 2013) would be necessary to

confirm this point. The second hypothesis is that there are several stages in the CO_2 dissolution mechanism and the number of CO_3^{2-} groups surrounding a Ca atom can be above 1. For instance, βMDE-5 glass with 1.7 wt.% CO_2 has a low Ca CN determined (8.0±0.6). For this particular sample investigated in Morizet et al. (2015), CO_2 molecules dissolve partially as Network CO_3^{2-} molecular groups (a CO_3^{2-} molecule intercalated between two tetrahedral units) whereas in RB8E-3 glass with 17.2 wt.% CO_2, CO_2 is only dissolved as Free Ionic Carbonate group as demonstrated by Morizet et al (2017b). The proposed chemical reaction to form Free Ionic Carbonates in Morizet et al. (2017c) based on ^{29}Si NMR results also suggests that more than one CO_2 molecule can be present in the surrounding of Ca atom and could explain the non-linear increase in the Ca CN.

As compared to Mg, the Ca structural environments in silicate glasses have longer bond length: ~2 Å for d_{Mg-O} and ~2.5 Å for d_{Ca-O}; and higher coordination values: <6 for Mg and >7 for Ca. From geometrical point of view, such differences could explain the preference of CO_2 molecules for dissolving in the vicinity of the Ca atoms rather than Mg atoms. Such a difference in the bond length to oxygen could also reflect a difference in the nature of the surrounding oxygen, either bridging (BO) or non-bridging (NBO). It has been shown (Kelsey et al., 2008; Stebbins, 2016) that Ca and Mg in silicate glasses are surrounded by both types of oxygens. For instance, Cormier and Cuello (2013) showed that increasing the #Mg induces an increase in the BO and a decrease in the NBO. Considering that CO_2 molecules scavenge NBOs to form free CO_3^{2-} groups in the investigated silicate glass compositions, therefore the lower concentration of NBO in the surrounding of the Mg atoms could prevent CO_2 molecules to dissolve close to Mg atoms.

5. Summary

It was recently suggested that CO_2 solubility in silicate glasses decreases with increasing #Mg and a possible explanation for that behaviour is either the lower affinity of CO_2 molecules for or a particular Mg atomic environment in silicate glasses. In the present study, we investigated CO_2-bearing silicate glasses using Mg and Ca K-edge XAS spectroscopy (XANES and EXAFS) at a synchrotron beamline. The studied glasses cover a wide range of chemical composition (from basalt to kimberlite) and a large range of CO_2 content (up to 17 wt.%), various synthesis conditions (P up to 3.0 GPa). For the investigated samples, the CO_2 dissolves as CO_3^{2-} molecular groups.

The XAS results show that the Mg atomic environments are not affected by the dissolution of CO_2 molecules whereas Ca atomic environments are changing upon CO_2 dissolution. These results corroborated the initial hypothesis which suggested that CO_2 molecules were dissolving preferentially in the Ca vicinity and not in the surrounding of the Mg atoms in silicate glasses.

The analysis of the fine structure with EXAFS revealed that the Ca coordination number is higher than the Mg coordination number in the structure and that it increases with increasing CO_2 content. The distance to the first neighbour is shorter for Mg than for Ca: ~2 Å for d_{Mg-O} and ~2.5 Å for d_{Ca-O}. Such geometrical differences could explain the CO_2 solubility behaviour as a function of #Mg. In other words, the Mg atomic environment in CO_2-bearing silicate glasses is too tight to allow the accommodation of CO_2 molecules in its surrounding.

Acknowledgement

The authors would like to thank the European Research Council who partly funded this work through the ERC project grant number 279790. The authors thank the University of Orléans, the University of Nantes and the CNRS for their access to analytical facilities. We thank the

anonymous reviewer for greatly improving the manuscript with interesting constructive criticisms and Don B. Dingwell for handling the manuscript. We acknowledge SOLEIL for provision of synchrotron radiation facilities on the LUCIA beamline and financial support for the project 20170041.

References

Andrault, D., Neuville, D. R., Flank, A.-M., Wang, Y., 1998. Cation sites in Al-rich $MgSiO_3$ perovskites. Am. Mineral. 83, 1045-1053.

Angeli, F., Gaillard, M., Jollivet, P., and Charpentier, T., 2007. Contribution of ^{43}Ca MAS NMR for probing the structural configuration of calcium in glass. Chem. Phys. Lett. 440, 324–328.

Binsted, N., Greaves, G.N., Henderson, C.M.B., 1985. An EXAFS study of glassy and crystalline phases of compositions $CaAl_2Si_2O_8$ (anorthite) and $CaMgSi_2O_6$ (diopside). Contrib. Mineral. Petrol. 89, 103-109.

Blanchard, P.E.R., Grosvenor, A.P., Rowson, J., Hughes, K., Brown, C., 2016. Identifying calcium-containing mineral species in the JEB Tailings Management Facility at McClean Lake, Saskatchewan. App. Geochem. 73, 98-108.

Blank, J.G., Brooker, R.A., 1994. Experimental studies of carbon dioxide in silicate melts: solubility, speciation and stable carbon isotope behaviour. In Volatiles in Magmas Reviews in Mineralogy, vol. 30 (eds. M. R. Carroll and J. R. Holloway). Mineral. Soc. Am., Washington, DC, pp. 157–186.

Bosshardt-Stadlin, S.A., Mattsson, H.B., Keller, J., 2014. Magma mixing and forced exsolution of CO_2 during the explosive 2007–2008 eruption of Oldoinyo Lengai (Tanzania). J. Volcanol. Geotherm. Res. 285, 229–246.

Brey, G., Ryabchikov, I., 1994. Carbon dioxide in strongly undersaturated melts and origin of kimberlitic magmas. N. Jb. Miner. Mh. H10, 449–463.

Brooker, R.A., Kohn, S.C., Holloway, J.R., McMillan, P.F., Carroll, M.R., 1999. Solubility, speciation and dissolution mechanisms for CO_2 in melts on the $NaAlO_2$-SiO_2 join. Geochim. Cosmochim. Acta 63, 3549-3565.

Brooker, R.A., Kohn, S.C., Holloway, J.R., McMillan, P.F., 2001a. Structural controls on the solubility of CO_2 in silicate melts. Part I: Bulk solubility data. Chem. Geol. 174, 225-240.

Brooker, R.A., Kohn, S.C., Holloway, J.R., McMillan, P.F., 2001b. Structural controls on the solubility of CO_2 in silicate melts. Part II: IR characteristics of carbonate groups in silicate glasses. Chem. Geol. 174, 241-254.

Brooker, R.A., Sparks, R.J.S., Kavanagh, J.L., Field, M., 2011. The volatile content of hypabyssal kimberlite magmas: some constraints from experiments on natural rock compositions. Bull. Volcanol.. http://dx.doi.org/10.1007/s00445-011-0523-7.

Cabaret, D., Sainctavit, P., Ildefonse, P., Flank, A.-M., 1998. Full multiple scattering calculations of the X-ray absorption near edge structure at the magnesium K-edge in pyroxene. Am. Mineral. 83, 300-304.

Cicconi, M.R., de Ligny, D., Gallo, T.M., Neuville, D.R., 2016. Ca neighbors from XANES spectroscopy: A tool to investigate structure, redox, and nucleation processes in silicate glasses, melts, and crystals. Am. Mineral. 101, 1232-1235.

Combes, J.-M., Brown Jr., G.E., Waychunas, G.A., 1991. X-ray absorption study of the local Ca environment in silicate glasses. In: Hasnain, S.S. (Ed.), X-ray Absorption Fine Structure, Proc. Sixth Int. Conf. on XAFS, York, pp. 312–314.

Cormier, L., Neuville, D.R., 2004. Ca and Na environment in Na_2O-CaO-Al_2O_3-SiO_2 glasses: influence of cation mixing and cation-network interactions. Chem. Geol. 213, 103–113.

Cormier, L., Cuello, G.J., 2013. Structural investigation of glasses along the $MgSiO_3$–$CaSiO_3$ join: Diffraction studies. Geochim. Cosmochim. Acta 122, 498-510.

Curti, E., Dähn, R., Farges, F., Vespa, M., 2009. Na, Mg, Ni and Cs distribution and speciation after long-term alteration of a simulated nuclear waste glass: A micro-XAS/XRF/XRD and wet chemical study. Geochim. Cosmochim. Acta 73, 2283-2298.

Davis, M.C., Sanders, K.J., Grandinetti, P.J., Gaudio, S.J., Sen, S., 2011. Structural investigations of magnesium silicate glasses by ^{29}Si 2D Magic-Angle Flipping NMR. J. Non-Cryst. Solids 357, 2787-2795.

Dixon, J. E., 1997. Degassing of alkalic basalts. Am. Mineral. 82, 368–378.

Du, X., Wu, M., Tse, J.S., Pan, Y., 2018. Structures and Transport Properties of $CaCO_3$ Melts under Earth's Mantle Conditions. Earth Space Chem. 2, 1-8.

Eggler, D.H., 1978. The effect of CO_2 upon partial melting of peridotite in the system Na_2O–CaO–Al_2O_3–MgO–SiO_2–CO_2 to 35 kb, with an analysis of melting in a peridotite-H_2O–CO_2 system. Am. J. Sci. 278, 305–343.

Fiske, P.S., Stebbins, J.F., 1994. The structural role of Mg in silicate liquids: A high-temperature ^{25}Mg, ^{23}Na and ^{29}Si NMR study. Am. Mineral. 79, 848-861.

Fleet, M.E., Liu, X., 2009. Calcium L2,3-edge XANES of carbonates, carbonate apatite, and oldhamite (CaS). Am. Mineral. 94, 1235-1241.

Gambuzzi, E., Pedone, A., Menziani, M.C., Angeli, F., Florian, P., Charpentier, T., 2015. Calcium environment in silicate and aluminosilicate glasses probed by ^{43}Ca MQMAS NMR experiments and MD-GIPAW calculations. Solid State Nuc. Mag. Res. 68-69, 31-36.

Guignard, M., Cormier, L., 2008. Environment of Mg and Al in $MgO–Al_2O_3–SiO_2$ glasses: a study coupling neutron and x-ray diffraction and reverse Monte Carlo modelling. Chem. Geol. 256, 111-118.

Iacono-Marziano, G., Morizet, Y., Le Trong, E., Gaillard, F., 2012. New experimental data and semi-empirical parameterization of $H_2O–CO_2$ solubility in mafic melts. Geochim. Cosmochim. Acta 97, 1–23.

Ildefonse, P., Calas, G., Flank, A.-M., Lagarde, P., 1995. Low Z elements (Mg, Al, and Si) K-edge X-ray absorption spectroscopy in minerals and disordered systems. Nucl. Instrum. Methods Phys. Res. B Beam Interact. Mater. Atoms 97, 172–175.

Jackson W.E., Farges, F., Yeager, M., Mabrouk, P.A., Rossano, S., Waychunas, G.A., Solomon, E.I., Brown, G.E.Jr., 2005. Multi-spectroscopic study of Fe(II) in silicate glasses: implications for the coordination environment of Fe(II) in silicate melts Geochim. Cosmochim. Acta 69, 4315–32

Kadik, A., Pineau, F., Litvin, Y., Jendrzejewski, N., Martinez, I., Javoy, M., 2004. Formation of carbon and hydrogen species in magmas at low oxygen fugacity. J. Petrol. 45, 1297–1310.

Kamenetsky, V.S., Grütter, H., Kamenetski, M.B., Gömann, K., 2013. Parental carbonatitic melt of the Koala kimberlite (Canada): Constraints from melt inclusions in olivine and Cr-spinel, and groundmass carbonate. Chem. Geol. 353, 96-111.

Katz, A.K., Glusker, J.P., BeeBe, S.A., Bock, C.W., 1996. Calcium ion coordination: A comparison with that of Beryllium, Magnesium, and Zinc. J. Am. Chem. Soc. 118, 5752-5763.

Kelsey, K.E., Allwardt, J.R., Stebbins, J.F., 2008. Ca-Mg mixing in aluminosilicate glasses: An investigation using the ^{17}O MAS and 3QMAS and ^{27}Al MAS NMR. J. Non-Cryst. Solids 354, 4644-4653.

Kelsey, K.E., Stebbins, J.F., Singer, D.M., Brown, G.E.J., Mosenfelder, J.L., Asimow, P.D., 2009. Cation field strength effects on high pressure aluminosilicate glass structure: Multinuclear NMR and La XAFS results. Geochim. Cosmochim. Acta 73, 3914-3933.

Kohara, S., Suzuya, K., Takeuchi, K., Loong, C.-K., Grimstditch, M., Weber, J.K.R., Tangeman, A., Key, S., 2004. Glass formation at the limit of insufficient network formers. Science 303, 1649–1652.

Kohara, S., Akola, J., Morita, H., Suzuya, K., Weber, J.K.R., Wilding, M.C., Benmore C.J., 2011. Relationship between topological order and glass forming ability in densely packed enstatite and forsterite composition glasses. Proc. Nat. Acad. Sci. 108, 14780-14785.

Kjarsgaard, B.A., Pearson, D.G., Tappe, S., Nowell, G.M., Dowall, D.P., 2009. Geochemistry of hypabyssal kimberlites from Lac de Gras, Canada: comparisons to a global database and applications to the parent magma problem. Lithos 1125, 236–248.

Kroeker, S., Stebbins, J.F., 2000. Magnesium coordination environments in glasses and minerals: new insight from high-field magnesium-25 MAS NMR. Am. Mineral. 85, 1459–1464.

le Roex, A.P., Bell, D.R., Davis, P., 2003. Petrogenesis of Group I kimberlites from Kimberley, South Africa: evidence from bulk-rock geochemistry. J. Petrol. 44, 2261–2286.

Li, D., Peng, M.S., Murata, T., 1999. Coordination and local structure of magnesium in silicate minerals and glasses: Mg K-edge XANES study. Can. Mineral. 37, 199–206.

Massuyeau, M., Gardés, E., Morizet, Y., Gaillard, F., 2015. A model for the activity of silica along the carbonatite–kimberlite–melilitite–basanite melt com-positional joint. Chem. Geol. 418, 206–216.

Mastelaro, V.R., Zanotto, E.D., 2018. X-ray Absorption Fine Structure (XAFS) Studies of Oxide Glasses—A 45-Year Overview. Materials 11, 204-244.

Morizet, Y., Brooker, R.A., Kohn, S.C., 2002. CO_2 in haplophonolite melt: solubility, speciation and carbonate complexation. Geochim. Cosmochim. Acta 66, 1809–1820.

Morizet, Y., Paris, M., Gaillard, F., Scaillet, B., 2010. C-O-H fluid solubility in haplobasalt under reducing conditions: An experimental study. Chem. Geol. 279, 1-16.

Morizet, Y., Brooker, R.A., Iacono-Marziano, G., Kjarsgaard, B., 2013. Quantification of CO_2 dissolved in silicate glasses of various compositions with Micro-Raman spectroscopy. Am. Mineral. 98, 1788-1802.

Morizet, Y., Paris, M., Gaillard, F., Scaillet, B., 2014a. Carbon dioxide in silica undersaturated melt. Part I: the effect of mixed alkalis (K and Na) on CO_2 solubility and speciation. Geochim. Cosmochim. Acta 141, 45–61.

Morizet, Y., Vuilleumier, R., Paris, M., 2015. A NMR and molecular dynamics study of CO_2-bearing basaltic melts and glasses. Chem. Geol. 418, 89-103.

Morizet, Y., Paris, M., Sifré, D., Di Carlo, I., Gaillard, F., 2017a. The effect of Mg concentration in silicate glasses on CO2 solubility and solution mechanism: implication for natural magmatic systems. Geochim. Cosmochim. Acta 198, 115–130.

Morizet, Y., Florian, P., Paris, M., Gaillard, F., 2017b. ^{17}O NMR evidence of free ionic clusters M^{n+} CO_3^{2-} in silicate glasses: Precursors for carbonate-silicate liquids immiscibility. Am. Mineral. 102, 1561-1564.

Morizet, Y., Paris, M., Sifré, D., Di Carlo, I., Ory, S., Gaillard, F., 2017c. Towards the reconciliation of viscosity change and CO_2-induced polymerization in silicate melts. Chem. Geol. 458, 38-47.

Mottana, A., Murata, T., Marcelli, A., Wu, Z.Y., Cibin, G., Paris, E., Giuli, G., 1999. The local structure of Ca-Na pyroxenes. II. XANES studies at the Mg and Al K-edges. Phys. Chem. Min. 27, 20-33.

Moulton, B.J.A., Henderson, G.S., Fukui, H., Hiraoka, N., de Ligny, D., Sonneville, C., Kanzaki, M., 2016. In situ structural changes of amorphous diopside ($CaMgSi_2O_6$) up to 20 GPa: A Raman and O K-edge X-ray Raman spectroscopic study. Geochim. Cosmochim. Acta 178, 41-61.

Mountjoy, G., 2007. The local atomic environment of oxygen in silicate glasses from molecular dynamics. J. Non-Cryst. Solids 353, 1849–1853.

Moussallam, Y., Morizet, Y., Massuyeau, M., Laumonier, M., Gaillard, F., 2015. CO_2 solubility in kimberlite melts. Chem. Geol. 418, 198-205.

Moussallam, Y., Florian, P., Corradini, D., Morizet, Y., Sator, N., Vuilleumier, R., Guillot, B., Iacono-Marziano, G., Schmidt, B.C., Gaillard, F., 2016. The molecular structure of melts along the carbonatite–kimberlite–basalt compositional joint: CO_2 and polymerization. Earth Planet. Science Lett. 434, 129-140.

Mysen, B.O., 1990. Effect of pressure, temperature, and bulk composition on the structure and species distribution in depolymerized alkali aluminosilicate melts and quenched melts. J. Geophys. Res. B 95, 15733–15744.

Mysen, B.O., Virgo, D., 1980a. Solubility mechanisms of carbon dioxide in silicate melts; a Raman spectroscopic study. Am. Mineral. 65, 885–899.

Neuville, D.R., Cormier, L., Flank, A.M., Briois, V., Massiot, D., 2004a. Al speciation and Ca environment in calcium aluminosilicate glasses and crystals by Al and Ca K-edge X‐ray absorption spectroscopy. Chem. Geol. 213, 153–163.

Neuville, D.R., de Ligny, D., Cormier, L., Henderson, G.S., Roux, J., Flank, A.-M., Lagarde, P., 2009. The crystal and melt structure of spinel and alumina at high temperature: An in-situ XANES study at the Al and Mg K-edge. Geochim Cosmochim Acta 73:3410-3422

Newman, S., Lowenstern, J.B., 2002. VolatileCalc: a silicate melt–H_2O–CO_2 solution model written in Visual Basic for excel, source. Comput. Geosci. 28, 597–604.

Newville, M., 2014. Fundamentals of XAFS. In Spectroscopic methods in mineralogy and material sciences Reviews in Mineralogy and Geochemistry, vol. 78 (eds. G.S. Henderson, D.R. Neuville and R.T. Downs). Mineral. Soc. Am., Washington, DC, pp. 33–74.

Paris, E., Wu, Z., Mottana, A., Marcelli, A., 1995. Calcium environment in omphacitic pyroxenes: XANES experimental data versus one electron multiple scattering calculations. Eur. J. Min. 7, 1065–1070.

Papale, P., Moretti, R., Barbato, D., 2006. The compositional dependence of the saturation surface of H_2O+CO_2 fluids in silicate melts. Chem. Geol. 229, 78–95.

Pawley, A.R., Holloway, J.R., McMillan, P.F., 1992. The effect of oxygen fugacity on the solubility of carbon–oxygen fluids in basaltic melt. Earth Planet. Science Lett. 110, 213–225.

Pohlenz, J., Rosa, A.D., Mathon, O., Pascarelli, S., Belin, S., Landrot, G., Murzin, V., Veligzhanin, A., Shiryaev, A., Irifune, T., Wilke, M., 2017. Structural controls of CO_2 on Y, La and Sr incorporation in sodium-rich silicate - carbonate melts by in-situ high P-T EXAFS. Chem. Geol. 486, 1-15.

Quartieri, S., Boscherini, F., Dalconi, C., Iezzi, G., Meneghini, C., Oberti, R., 2008. Magnesium K-edge EXAFS study of bond-length behavior in synthetic pyrope-grossular garnet solid solutions. Am. Mineral. 93, 495-498.

Ragoen, C., Cormier, L., Bidegaray, A.–I., Vives, S., Henneman, F., Trcera, N., Godet, S., 2017. A XANES investigation of the network-modifier cations environment before and after the Na+/K+ ion-exchange in silicate glasses. J Non-Cryst. Solids 479, 97-104.

Ravel, B., Newville, M., 2005. ATHENA, ARTHEMIS, HEPHAESTUS: data analysis for X-ray absorption spectroscopy using IFEFFIT. J. Synch. Rad. 12, 537–541.

Russell, J.K., Porritt, L.A., Lavallée, Y., Dingwell, D.B., 2012. Kimberlite ascent by assimilation-fuelled buoyancy. Nature 481, 352–356.

Shimoda, K., Tobu, Y., Hatakeyama, M., Nemoto, T., Saito, K., 2007. Structural investigation of Mg local environments in silicate glasses by ultra-high field ^{25}Mg 3QMAS NMR spectroscopy. Am. Mineral. 92, 695-698.

Shimoda, K., Nemoto, T., Saito, K., 2008a. Local Structure of Magnesium in Silicate Glasses: A ^{25}Mg 3QMAS NMR Study. J. Phys. Chem. B 112, 6747-6752.

Shimoda, K., Tobu, Y., Kanehashi, K., Nemoto, T., Saito, K., 2008b. Total understanding of the local structures of an amorphous slag: Perspective from multi-nuclear (^{29}Si, ^{27}Al, ^{17}O, ^{25}Mg, and ^{43}Ca) solid-state NMR. J. Non-Cryst. Solids 354, 1036-1043.

Skinner, L.B., Benmore, C.J., Weber, J.K.R., Tumber, S., Lazareva, L., Neuefeind, J., Santodonato, L., Du, J., Parise, J.B., 2012. Structure of Molten $CaSiO_3$: Neutron Diffraction Isotope Substitution with Aerodynamic Levitation and Molecular Dynamics Study. J Phys. Chem. B 116, 13439-13447.

Sowrey, F.E., Skipper, L.J., Pickup, D.M., Drake, K.O., Lin, Z., Smith, M.E., Newport, R.J., 2004. Systematic empirical analysis of calcium–oxygen coordination environment by calcium K-edge XANES. Phys. Chem. Chem. Phys. 6, 188–192.

Stebbins, J.F., 2016. Glass structure, melt structure, and dynamics: Some concepts for petrology. Am. Mineral. 101, 753-768.

Taniguchi, T., Okuno, M., Matsumoto, T., 1997. X-ray diffraction and EXAFS studies of silicate glasses containing Mg, Ca and Ba atoms. J Non-Cryst. Solids 211, 56-63.

Thibault, Y., Holloway, J.R., 1994. Solubility of CO_2 in a Ca-rich leucitite: effects of pressure, temperature and oxygen fugacity. Contrib. Miner. Petrol. 116, 216–224.

Trcera, N., Cabaret, D., Rossano, S., Farges, F., Flank, A.-M., Lagarde, P., 2009. Experimental and theoretical study of the structural environment of magnesium in minerals and silicate glasses using x-ray absorption near-edge structure Phys. Chem. Miner. 36, 241–57.

Trcera, N., Rossano, S., Madjer, K., Cabaret, D., 2011. Contribution of molecular dynamics simulations and ab initio calculations to the interpretation of Mg K-edge experimental XANES in K_2O–MgO–$3SiO_2$ glass. J. Phys. Condens. Matter 23, 255401-255409.

Vuilleumier, R., Sator, N., Guillot, B., 2009. Computer modelling of natural silicate melts: what can we learn from ab initio simulations. Geochim. Cosmochim. Acta 73, 6313-6339.

Wetzel, D.T., Rutherford, M.J., Jacobsen, S.D., Hauri, E.H., Saal, A.E., 2013. Degassing of reduced carbon from planetary basalts. Proc. Nat. Acad. Sci. doi/10.1073/pnas.1219266110

Wilding, M.C., Benmore, C.J., Tangeman, J.A., Sampath, S., 2004. Coordination changes in magnesium silicate glasses. Europhys. Lett. 67, 212–218.

Wilding, M.C., Benmore, C.J., Weber, J.K.R., 2008. In situ diffraction studies of magnesium silicate liquids. J. Mater. Sci. 43, 4707-4713.

Wilding, M., Guthrie, M., Kohara, S., Bull, C.L., Akola, J., Tucker, M.G., 2012. The structure of $MgO–SiO_2$ glasses at elevated pressure. J. Phys. Condens. Matter 24, 225403-225414.

Yoshimura, T., Tamenori, Y., Iwasaki, N., Hasegawa, H., Suzuki, A., Kawahata, H., 2013. Magnesium K-edge XANES spectroscopy of geological standards. J. Synch. Rad. 20, 734-740.

Figure caption

Figure 1: XAS spectra obtained at the Mg K-edge for crystalline materials (spinel and periclase) and CO_2-bearing silicate glasses: A, for depolymerized (NBO/T > 2) kimberlite glasses; B, for moderately depolymerized (NBO/T = 1) haplobasalt synthesized at 1.5 GPa. The CO_2 content, synthesis pressure, degree of polymerization (NBO/T) and #Mg are reported next to each spectrum. The spectra can be decomposed into two regions: XANES up to ~1340 eV and the EXAFS region above 1340 eV. Crystalline compounds exhibit five features denoted *A* to *E*, whereas silicate glasses only show four peak from *a* to *d*.

Figure 2: XAS spectra obtained at the Ca K-edge for crystalline materials (diopside and dolomite) and CO_2-bearing silicate glasses: A, for depolymerized (NBO/T > 2) melilitite and kimberlite glasses, the spectrum for CO_2-free wollastonite has also been added; B, for moderately depolymerized (NBO/T = 1) haplobasalt synthesized at 1.5 GPa. The CO_2 content, synthesis pressure, degree of polymerization (NBO/T) and #Mg are reported next to each spectrum. The spectra can be decomposed into two regions: XANES up to ~4075 eV and the EXAFS region above 4075 eV. As inferred in previous works (see references in the text), several features can be distinguished in the spectra for silicate glasses and denoted *p* corresponding to the pre-edge peak and *a* to *c*.

Figure 3: Change in the main line of the Ca and Mg XANES spectrum as a function of CO_2 content. A 10% in relative to the value for the wt.% CO_2 and ±0.1 eV for the absorption energy are considered.

Figure 4: Calculated d_{Mg-O} distance in Å using the model of Li et al. (1999) as a function of the experimentally determined Mg K-edge in eV. The d_{Mg-O} is reported for the analysed crystalline compounds and CO_2-bearing silicate glasses.

Figure 5: A) Normalized k^3-weighted Mg K-edge EXAFS $\chi(k)$ and fit for X3-2 silicate glass; B) Magnitude $\chi(R)$ in $Å^{-3}$ in the R-space for X3-2 silicate glass; C) Normalized k^3-weighted Mg K-edge EXAFS $\chi(k)$ and fit for HKM silicate glass; D) Magnitude $\chi(R)$ in $Å^{-3}$ in the R-space for HKM silicate glass. The fit of the k^3-weighted $\chi(k)$ and the magnitude $\chi(R)$ in the R-space were done between 2 and 7.1 $Å^{-1}$ and 1 and 2.2 Å, respectively. We used a one Mg to O single scattering path from periclase crystallographic structure to fit the Mg EXAFS signal.

Figure 6: A) Normalized k^2-weighted Ca K-edge EXAFS $\chi(k)$ and fit for TA12-C3 silicate glass; B) Magnitude $\chi(R)$ in $Å^{-4}$ in the R-space for TA12-C3 silicate glass; C) Normalized k^2-weighted Ca K-edge EXAFS $\chi(k)$ and fit for X3-2 silicate glass; D) Magnitude $\chi(R)$ in $Å^{-4}$ in the R-space for X3-2 silicate glass. The fit of the k^2-weighted $\chi(k)$ and the magnitude $\chi(R)$ in the R-space were done between 2 and 8 $Å^{-1}$ and 1 and 3 Å, respectively. We used a three Ca to O single scattering paths and single Ca to Si scattering path from diopside crystallographic structure to fit the Ca EXAFS signal.

Figure 7: Change in the Ca coordination number (CN) as a function of CO_2 content (in wt.%) for silicate glasses. The Ca CN is determined from the subsequent Ca EXAFS simulations shown in Figure 6. The error on the CO_2 content is 10% in relative to the value and the error on the Ca CN is determined from error propagation obtained from the Ca EXAFS fit.

Table caption:

Table 1: Sample composition (major elements and volatiles), synthesis conditions and chemical parameters (NBO/T and XMg).

Table 2: Mg and Ca K-edge XAS results for CO_2-bearing silicate glasses: XANES peak maximum, EXAFS simulation results (Mg and Ca coordination numbers, calculated distance to first neighbour).

Table 1

Sample	Temperature (°C)	Pressure (GPa)	SiO_2 (wt.%)[a]	Al_2O_3	FeO	MgO	CaO	Na_2O	K_2O	CO_2[b]	NBO/T[c]	XMg[d]
Woll	1500	0.0001	51.7	0	0	0	48.3	0	0	0	2	0
HK-1	1550	1.5	40.2	4.3	0.0	21.9	22.0	4.5	0.0	7.1	2.6	0.58
HK-2	1550	0.5	40.1	4.4	0.0	21.3	22.3	4.5	0.0	5.6	2.5	0.57
HK-3	1550	1.0	37.2	4.2	0.0	21.8	21.4	4.5	0.0	2.9	2.7	0.59
HKM	1550	1.5	31.8	3.5	0.0	21.9	22.0	3.5	0.0	13.2	3.2	0.58
RB8E-3	1550	1.5	30.1	8.7	0.0	0.2	39.4	5.5	0.0	17.2	1.9	0
RB8-2	1550	0.5	33.2	9.8	0.3	0.2	40.4	4.9	0.0	6.0	2.1	0
X1-2	1525	1.5	39.7	14.2	0.1	6.0	25.1	4.8	0.0	7.5	1.1	0.25
BX2	1525	1.5	42.0	15.4	0.7	12.3	17.5	4.8	0.0	3.6	1.2	0.50
X3-2	1525	1.5	43.1	16.1	0.0	17.6	12.0	5.2	0.0	1.5	1.1	0.67
βMDE-5	1550	2.0	48.9	17.4	0.0	17.4	16.3	0.0	0.0	1.7	1.0	0.60
TA12-C1	1400	1.0	42.5	9.5	3.2	9.6	21.2	0.8	5.8	3.7	1.4	0.39
TA12-C3	1400	3.0	38.6	8.8	3.8	8.8	20.1	0.7	5.8	10.5	1.5	0.38
TA10b-C1	1400	1.0	26.9	6.3	1.4	19.7	26.2	0.5	3.6	12.9	3.4	0.51
TA10b-CH1	1400	1.0	26.6	6.1	1.6	19.5	26.0	0.5	3.6	12.7	3.4	0.51

[a] The glass composition was determined by EPMA analyses and has been reported in previous studies. The observed error based on replicated EPMA analyses associated to each oxide concentration is less 0.2 wt.% in relative.

[b] The CO_2 solubility has been determined using the method of Morizet et al. (2013) and using the derived CO3/HF value obtained from the deconvolution of the Raman spectra. The associated error on the CO_2 content using this Raman method is 10% in relative to the value.

[c] The NBO/T corresponds to the concentration of Non-Bridging Oxygen per Tetrahedron and is calculated from the chemical composition (Mysen, 1990).

[d] The XMg is defined as molar ratio MgO/(MgO+CaO).

Table 2

Sample	CO_2	Mg XANES		Mg EXAFS[c]		Ca XANES	Ca EXAFS[c]	
		Peak maximum (eV)[a]	Calc. dMg-O (Å)[b]	Calc. dMg-O (Å)	Mg CN	Peak maximum (eV)[a]	Calc dCa-O (Å)	Ca CN
Woll	0					4051.4	2.54±0.24	7.1±0.5
HK-1	7.1	1309.8	1.96	2.04±0.05	3.7±1.3	4050.9	2.52±0.51	9.1±1.3
HK-2	5.6	1309.7	1.96	2.01±0.01	6.1±0.5	4051.1	2.49±0.32	8.8±0.9
HK-3	2.9	1309.6	1.95	2.00±0.01	5.6±0.5	4051.0	2.53±0.31	8.9±0.9
HKM	13.2	1310.4	2.01	2.00±0.01	5.7±0.6	4050.8	2.50±0.31	9.0±0.8
RB8E-3	17.2					4050.9	2.53±0.23	9.3±0.4
RB8-2	6.0					4050.9	2.55±0.39	9.5±1.1
X1-2	7.5	1309.8	1.96	1.98±0.00	6.0±0.2	4051.0	2.51±0.42	9.3±1.3
BX2	3.6	1309.9	1.97	2.01±0.02	5.9±0.6	4051.1	2.53±0.28	8.9±0.8
X3-2	1.5	1309.9	1.97	1.98±0.01	6.0±0.3	4051.2	2.53±0.43	8.6±1.1
βMDE-5	1.7	1309.8	1.96	2.00±0.01	5.6±0.4	4051.2	2.50±0.23	8.0±0.6
TA12-C1	3.7					4051.1	2.48±0.26	8.4±0.6
TA12-C3	10.5	1310.1	1.98	2.00±0.01	6.2±0.5	4050.8	2.51±0.41	9.3±1.2
TA10b-C1	12.9	1309.5	1.94	1.99±0.01	5.5±0.4	4051.0	2.51±0.24	9.1±0.7
TA10b-CH1	12.7	1309.4	1.94	1.99±0.02	6.5±0.9	4051.0	2.48±0.26	9.2±0.7

[a] The peak maximum corresponds to the peak maximum of the main line *b* and has been determined from the simulation of the XANES region. The error on the peak is 0.2 eV.

[b] The d_{Mg-O} in Å has been calculated from the model of Li et al. (1999) relating the position of the Mg K-edge to the distance between Mg and O atoms in the first coordination sphere.

[c] The Mg and Ca EXAFS results (distance to O and CN) were obtained from the simulation of the oscillatory EXAFS signal (see Figure 5 and 6) and using the Artemis software (Ravel and Newville, 2005). The error on each parameter is calculated from error propagation method.

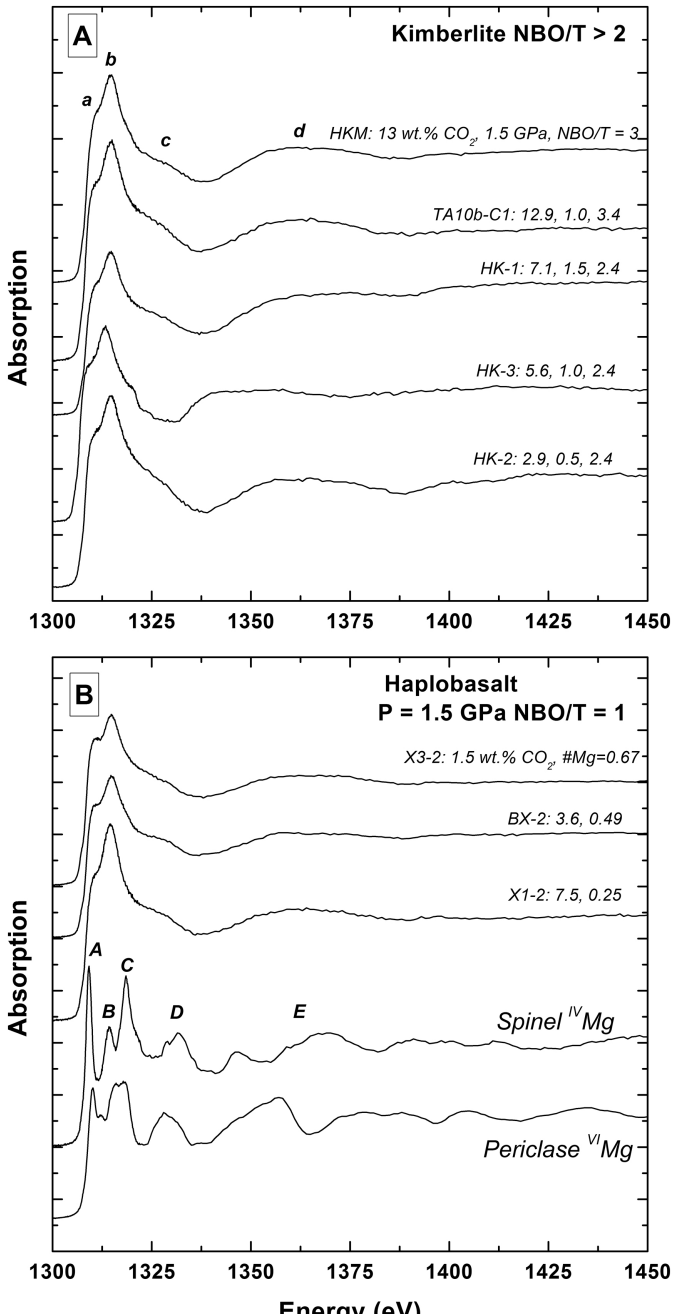
A
Kimberlite NBO/T > 2
a
b
c
d
HKM: 13 wt.% CO2, 1.5 GPa, NBO/T = 3
TA10b-C1: 12.9, 1.0, 3.4
HK-1: 7.1, 1.5, 2.4
HK-3: 5.6, 1.0, 2.4
HK-2: 2.9, 0.5, 2.4
Absorption
1300
1325
1350
1375
1400
1425
1450
B
Haplobasalt
P = 1.5 GPa NBO/T = 1
X3-2: 1.5 wt.% CO2, #Mg=0.67
BX-2: 3.6, 0.49
X1-2: 7.5, 0.25
A
B
C
D
E
Spinel IVMg
Periclase VIMg
Absorption
1300
1325
1350
1375
1400
1425
1450
Energy (eV)

Figure 1

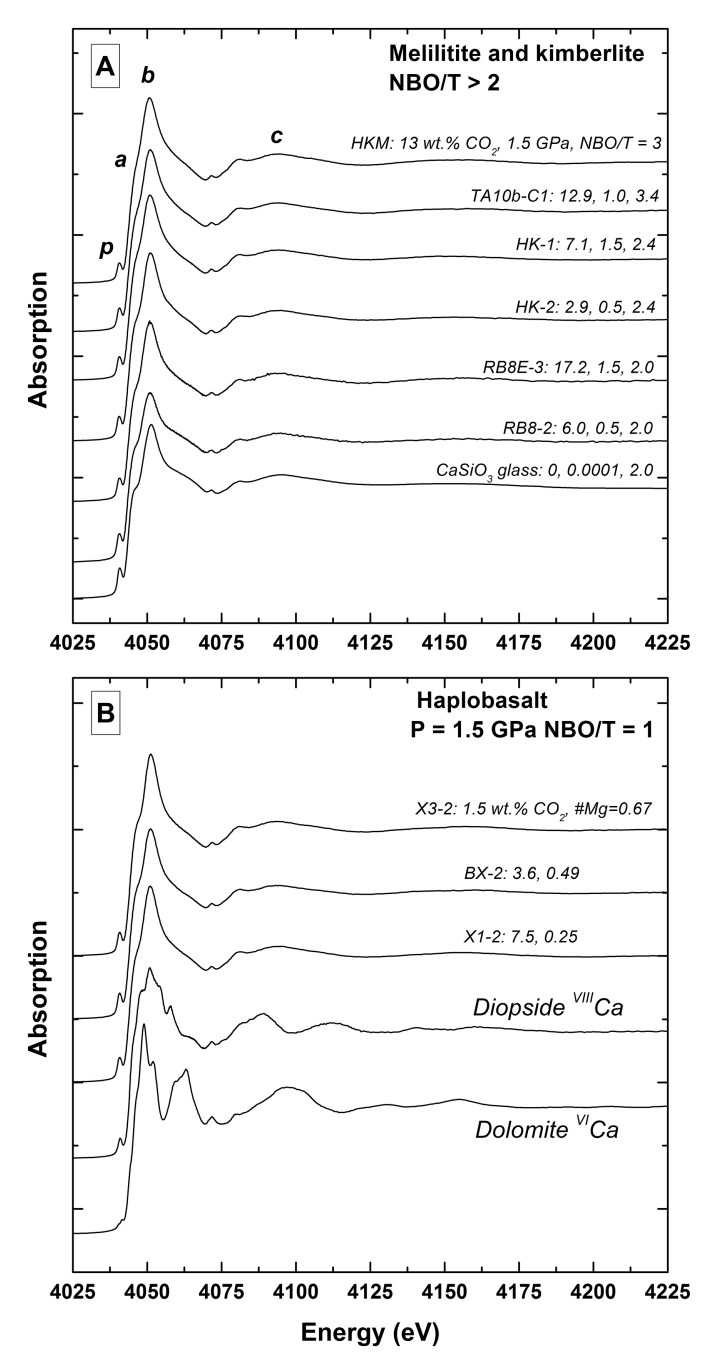
A
Melilitite and kimberlite
NBO/T > 2
b
a
p
c
HKM: 13 wt.% CO2, 1.5 GPa, NBO/T = 3
TA10b-C1: 12.9, 1.0, 3.4
HK-1: 7.1, 1.5, 2.4
HK-2: 2.9, 0.5, 2.4
RB8E-3: 17.2, 1.5, 2.0
RB8-2: 6.0, 0.5, 2.0
CaSiO3 glass: 0, 0.0001, 2.0
Absorption
4025 4050 4075 4100 4125 4150 4175 4200 4225
B
Haplobasalt
P = 1.5 GPa NBO/T = 1
X3-2: 1.5 wt.% CO2, #Mg=0.67
BX-2: 3.6, 0.49
X1-2: 7.5, 0.25
Diopside VIIICa
Dolomite VICa
Absorption
4025 4050 4075 4100 4125 4150 4175 4200 4225
Energy (eV)

Figure 2

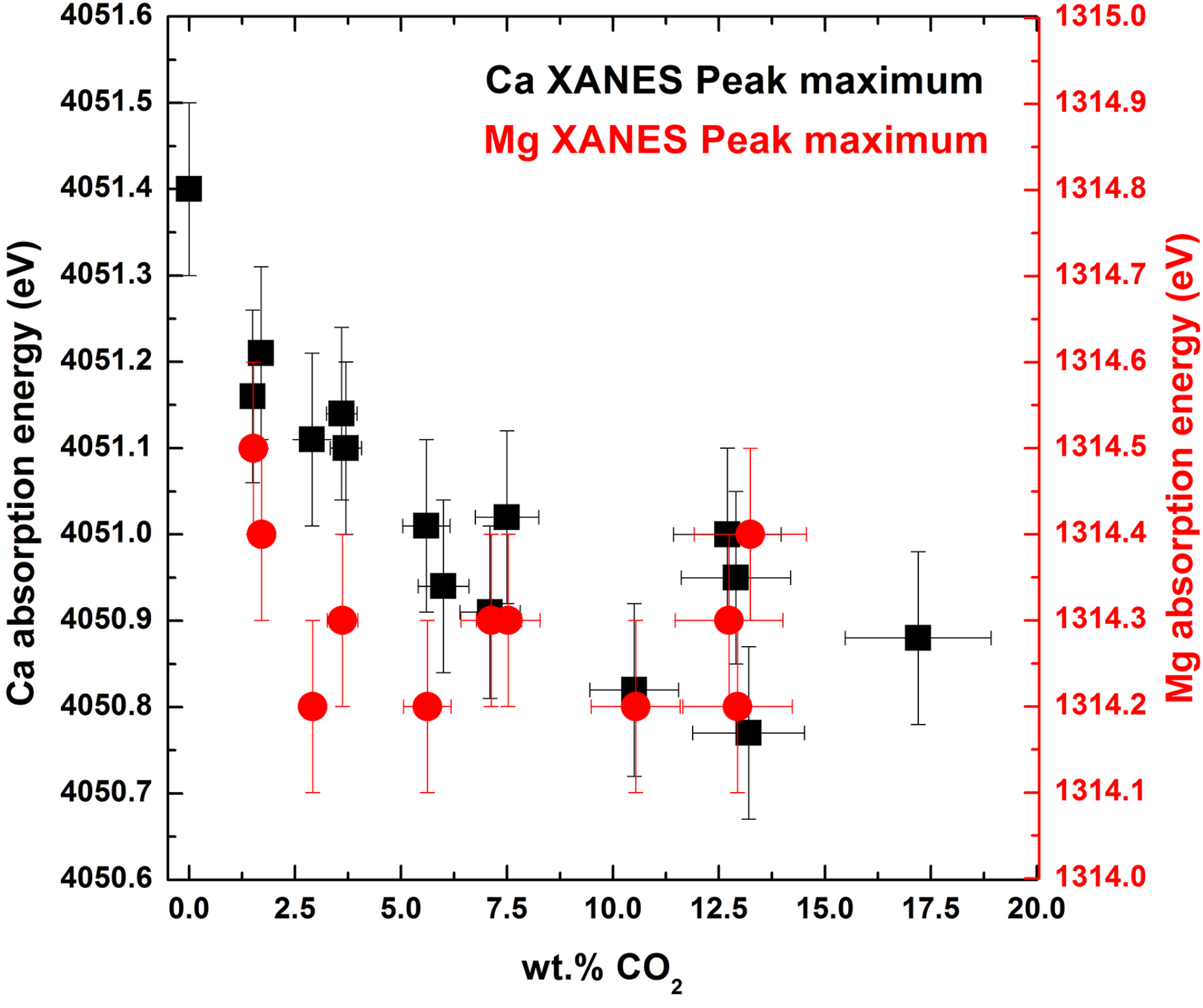
Ca XANES Peak maximum
Mg XANES Peak maximum
Ca absorption energy (eV)
Mg absorption energy (eV)
wt.% CO2
4051.6
4051.5
4051.4
4051.3
4051.2
4051.1
4051.0
4050.9
4050.8
4050.7
4050.6
1315.0
1314.9
1314.8
1314.7
1314.6
1314.5
1314.4
1314.3
1314.2
1314.1
1314.0
0.0
2.5
5.0
7.5
10.0
12.5
15.0
17.5
20.0

Figure 3

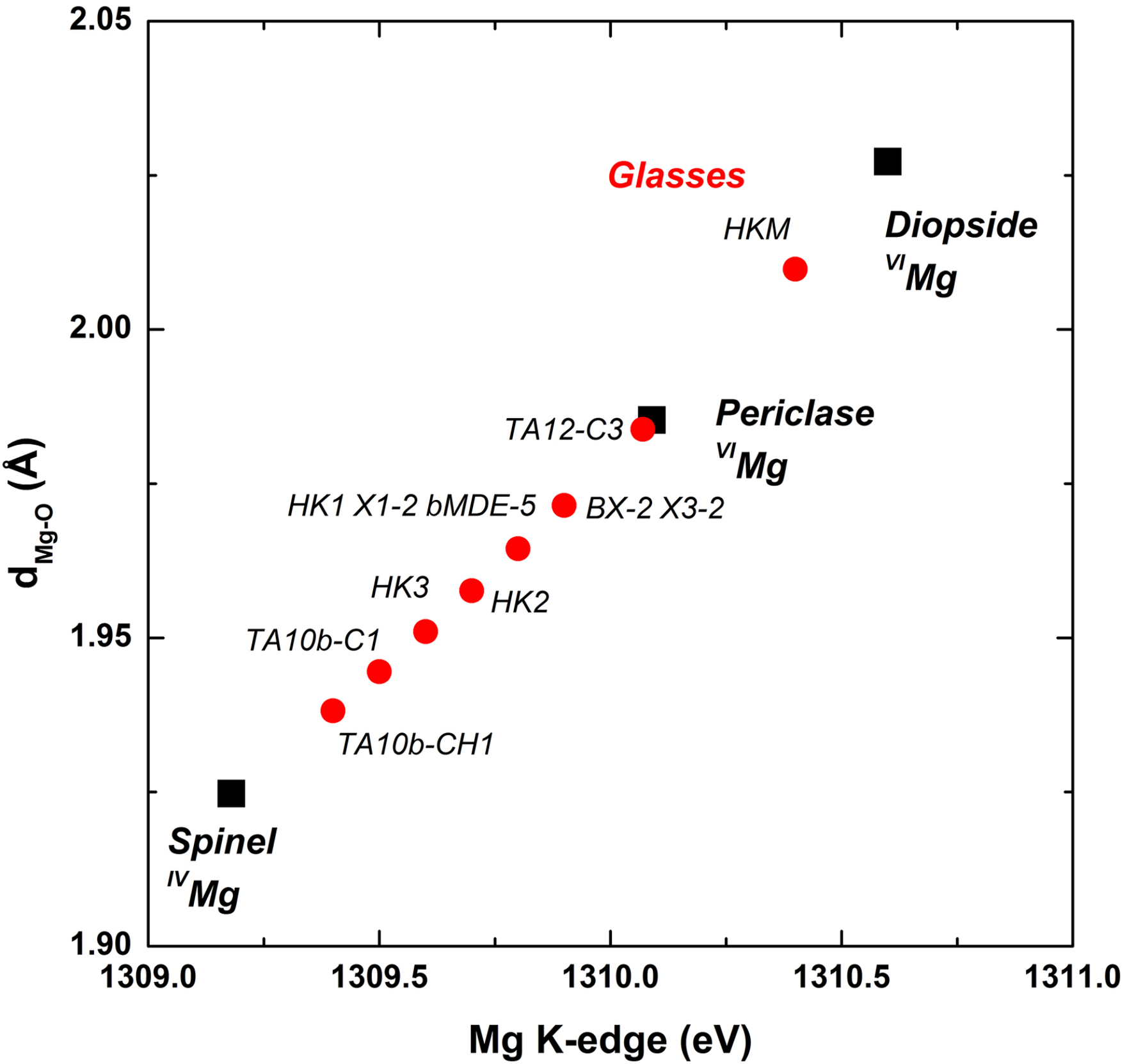
2.05
2.00
1.95
1.90
1309.0
1309.5
1310.0
1310.5
1311.0
Mg K-edge (eV)
d Mg-O (Å)
Glasses
HKM
Diopside
VI Mg
TA12-C3
Periclase
VI Mg
HK1 X1-2 bMDE-5
BX-2 X3-2
HK3
HK2
TA10b-C1
TA10b-CH1
Spinel
IV Mg

Figure 4

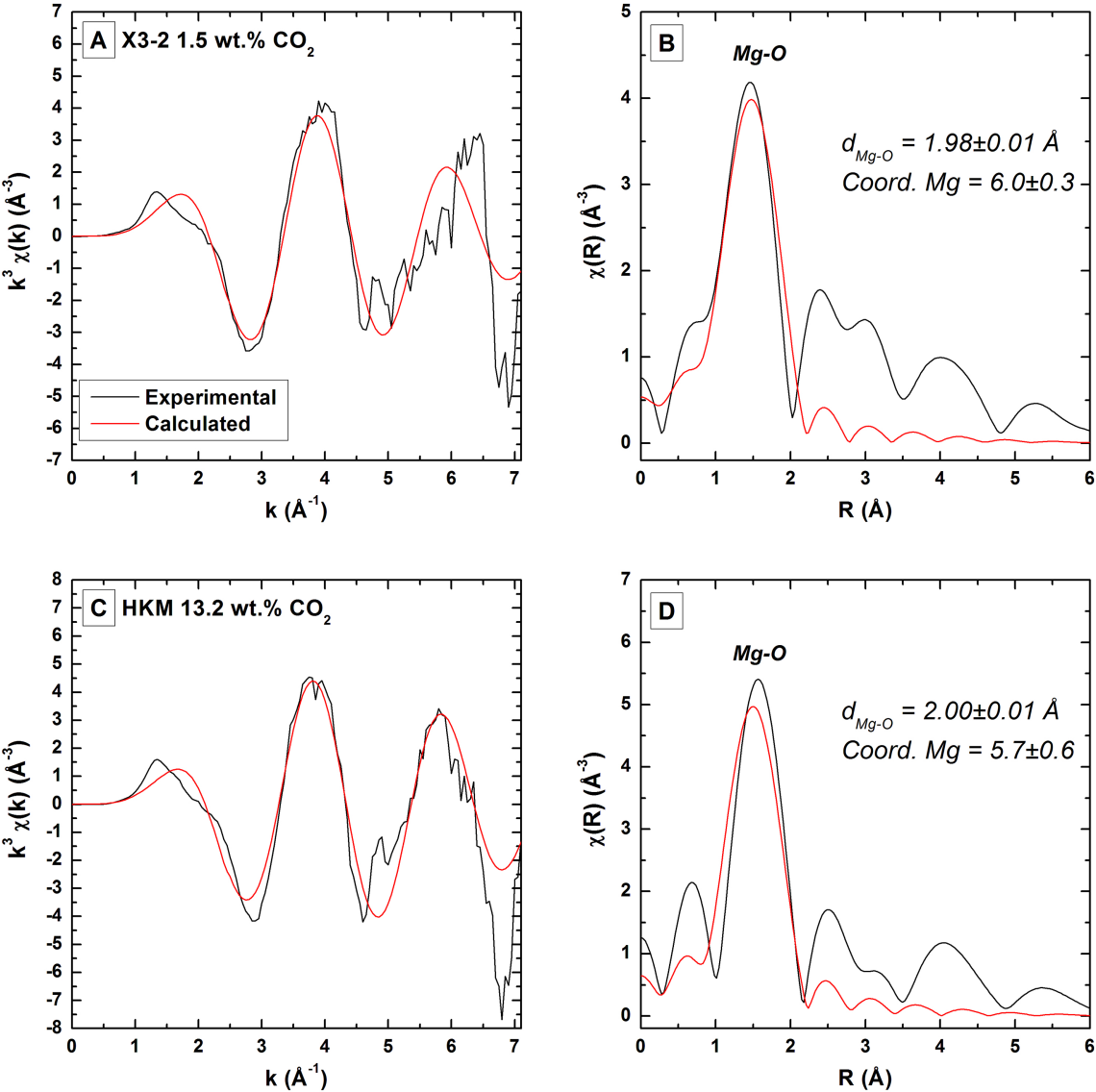
A
X3-2 1.5 wt.% CO2
Experimental
Calculated
k3 χ(k) (Å-3)
k (Å-1)
B
Mg-O
dMg-O = 1.98±0.01 Å
Coord. Mg = 6.0±0.3
χ(R) (Å-3)
R (Å)
C
HKM 13.2 wt.% CO2
k3 χ(k) (Å-3)
k (Å-1)
D
Mg-O
dMg-O = 2.00±0.01 Å
Coord. Mg = 5.7±0.6
χ(R) (Å-3)
R (Å)

Figure 5

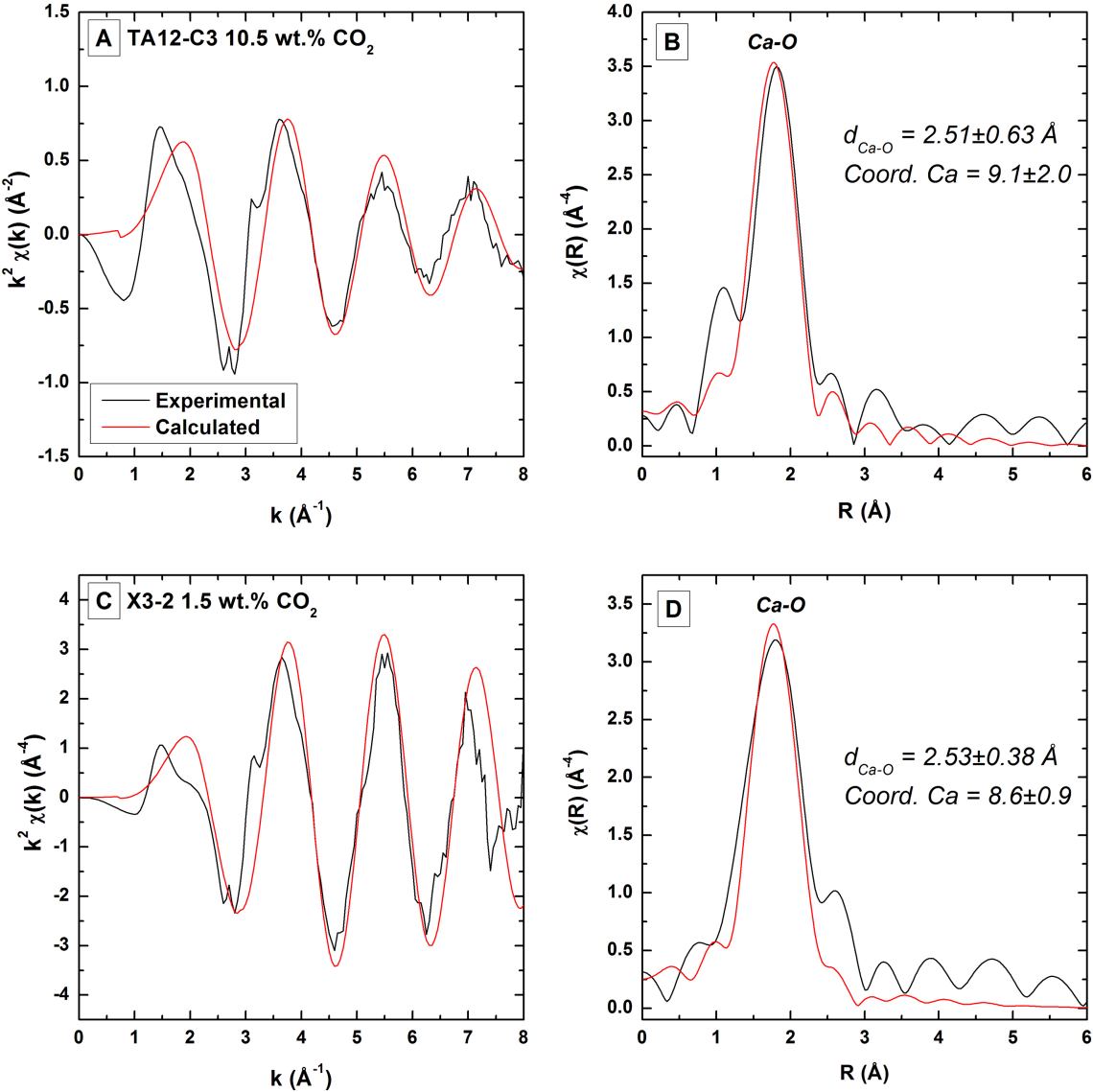
A
TA12-C3 10.5 wt.% CO2
Experimental
Calculated
k2 χ(k) (Å-2)
k (Å-1)
B
Ca-O
dCa-O = 2.51±0.63 Å
Coord. Ca = 9.1±2.0
χ(R) (Å-4)
R (Å)
C
X3-2 1.5 wt.% CO2
k2 χ(k) (Å-4)
k (Å-1)
D
Ca-O
dCa-O = 2.53±0.38 Å
Coord. Ca = 8.6±0.9
χ(R) (Å-4)
R (Å)

Figure 6

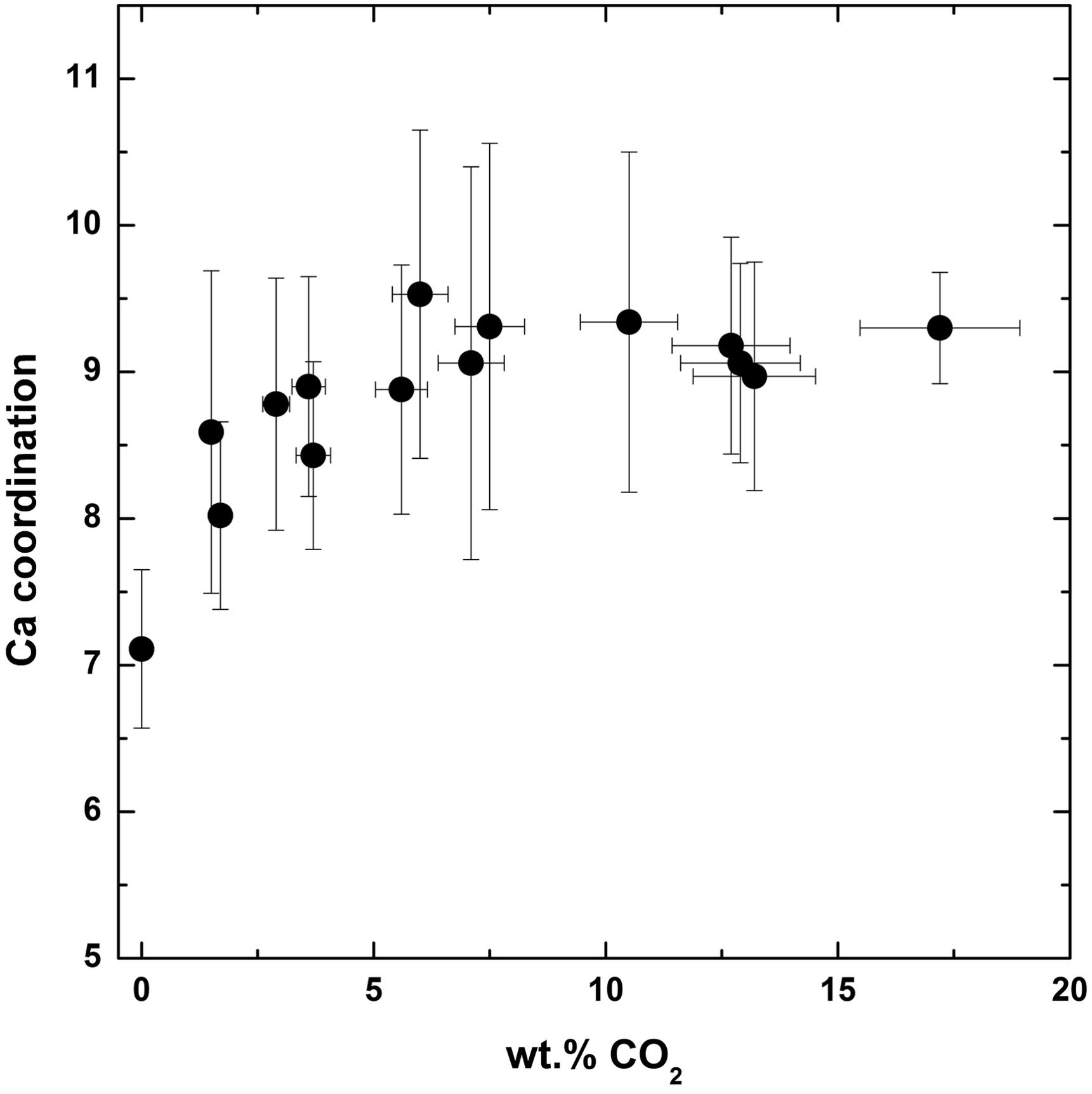

Figure 7